Lawrence Berkeley National Laboratory
Recent Work

Title
STRUCTURE AND MECHANICAL PROPERTIES OF Cu-Mn-Al ALLOY

Permalink
https://escholarship.org/uc/item/9bq7v07m

Author
Mirmirani, Fereshteh Samimi.

Publication Date
1974-04-01

eScholarship.org Powered by the California Digital Library
University of California

LBL-2598

STRUCTURE AND MECHANICAL PROPERTIES OF Cu-Mn-Al ALLOY

Fereshteh Samimi Mirmirani
(M.S. thesis)

RECEIVED
LAWRENCE
RADIATION LABORATORY

JUN 12 1974

LIBRARY AND
DOCUMENTS SECTION

April 1974

Prepared for the U. S. Atomic Energy Commission
under Contract W-7405-ENG-48

TWO-WEEK LOAN COPY

This is a Library Circulating Copy which may be borrowed for two weeks. For a personal retention copy, call Tech. Info. Division, Ext. 5545

LBL-2598

DISCLAIMER

This document was prepared as an account of work sponsored by the United States Government. While this document is believed to contain correct information, neither the United States Government nor any agency thereof, nor the Regents of the University of California, nor any of their employees, makes any warranty, express or implied, or assumes any legal responsibility for the accuracy, completeness, or usefulness of any information, apparatus, product, or process disclosed, or represents that its use would not infringe privately owned rights. Reference herein to any specific commercial product, process, or service by its trade name, trademark, manufacturer, or otherwise, does not necessarily constitute or imply its endorsement, recommendation, or favoring by the United States Government or any agency thereof, or the Regents of the University of California. The views and opinions of authors expressed herein do not necessarily state or reflect those of the United States Government or any agency thereof or the Regents of the University of California.

STRUCTURE AND MECHANICAL PROPERTIES OF
Cu-Mn-Al ALLOY

Contents

STRUCTURE AND MECHANICAL PROPERTIES OF Cu-Mn-Al ALLOY

Fereshteh Samimi Mirmirani

Inorganic Materials Research Division, Lawrence Berkeley Laboratory and Department of Materials Science and Engineering, College of Engineering; University of California, Berkeley, California 94720

ABSTRACT

A $Cu_{2.5}Mn_{0.5}Al$ alloy having the symmetrical composition near the center of the miscibility gap, was heat treated to produce spinodal structures with various wavelengths. Transmission electron microscopy and diffraction were used to study the spinodally decomposed microstructures, to measure the wavelength, and the difference of the lattice parameters of the precipitating phases. The latter was also measured by X-ray diffraction.

The microstructural changes upon ageing at different temperatures were correlated with hardness measurements. The latter were used because of the brittleness of the alloy. The Vickers hardness did not correlate well with wavelength and difference in lattice parameter changes as some theories predict, but appears to be controlled by the $L1_0 \rightarrow DO_3$ transformation within the binary rich phase at least up to the maximum in hardness. The rate of coarsening of the major phases (Cu_3Al and Cu_2MnAl) also appears to be modified by the presence of $L1_0$ particles, since deviations from the classical coarsening rates were observed.

I. INTRODUCTION

Spinodal decomposition is a mechanism of phase transformation which is homogeneous in character and consequently is promising for applications in certain metallic systems to produce homogeneous microstructures, and more uniformity in mechanical properties. The theoretical aspects of spinodal transformations have been reviewed and summarized (e.g., Cahn[1,2] and Hilliard[3]), and are now quite well understood. Spinodal decomposition is characterized by small composition fluctuations over large distances, producing a microstructure which can be characterized by three parameters, volume fraction of the phases, amplitude, and wavelength of the fluctuations. An analysis of these parameters in spinodal Cu-Ni-Fe alloys has been performed by Livak and Thomas.[4] Their experimental results revealed that, while coherency is maintained, the yield stress is directly proportional to the difference in cubic lattice parameters of the two precipitating phases, and is independent of the wavelength and volume fractions.

The metallography of the $(Cu\text{-}Mn)_3Al$ system which also gives evidence of spinodal decomposition has been investigated by Bouchard and Thomas.[5-8] They studied quenched and aged alloys along the composition tie line Cu_3Al-Cu_2MnAl by electron diffraction and microscopy (Fig. 1). Their study showed that, the Cu_2MnAl Heusler alloy has an ordered body centered cubic structure. During the quench, ordering occurs, forming a solid solution based on the DO_3 structure of Cu_3Al and the $L2_1$ structure of Cu_2MnAl (Fig. 2). By aging below 350°C, the alloy decomposes to Cu_2MnAl and Cu_2Al, and the microstructure possesses all the metallographic

characteristics of spinodal decomposition. Cu_3Al rich and Cu_2MnAl rich modulations posses the DO_3 and L2, structures at temperatures near the top of the miscibility gap. However, at lower temperatures, the Cu_3Al rich modulations also give diffraction evidence for the existence of a tetragonal structure believed to be similar to the $L1_0$ superstructure. The transformation $DO_3 \rightarrow L1_0$ was studied by Thomas and Bouchard[7] who suggested that the transformation can be accomplished by the ordering of only one set of the {220} type planes in the DO_3 structure, but other possibilities can be considered.[9] Assuming that the binary rich phase has the Cu_3Al composition and is stable below 375°C, at 300°C it is metastable. The electron diffraction patterns then show diffuse streaking and extra reflections which can be indexed in terms of the $L1_0$ structure. At this aging condition the morphology of the Cu_3Al rich modulation shows the "tweed" texture in electron micrographs.[10] There are twelve possible $L1_0$ variants that can be classified into three sets of twin related variants coherent with their APB related counterparts. The $L1_0$ structure consists of the planes parallel to a {110} plane of the matrix and twin related variants can concurrently grow in platelets parallel to the {100} planes of the matrix.

The transformations are shown schematically in Fig. 2. It can be seen that the aging characteristics of the CuMnAl alloys are very complex and no work has been published so far on correlating the aging with mechanical properties. Consequently the objective of this investigation is to determine experimentally the effect of aging on the mechanical properties and structure of an alloy having the symmetrical composition $Cu_{2.5}Mn_{0.5}Al$. For this purpose, the two parameters, wavelength and amplitude, have

been studied. The changes in microstructure and wavelength with aging time have been followed by transmission electron microscopy and diffraction. The changes in Δa (the differences in lattice parameter of the two decomposed phases) have been determined from the separation of spots in selected area diffraction patterns. X-ray diffraction was used to verify the accuracy of the Δa measurements by electron diffraction. In addition, Curie temperature measurements, which are a function of composition of the ferromagnetic Cu_2MnAl rich phase, have been made to determine the amplitude of the composition fluctuations. In order to establish the yield stress, a widely used criterion of mechanical behavior, both tensile and compression tests have also been conducted. However, because of the extensive brittleness of the alloy, tensile mechanical properties could not be measured, so Vicker's hardness was used as an indication of the variation in strength with aging, and mostly Vicker's hardness was used to gage the property changes.

The oil quenched specimens were chosen for subsequent aging treatment based on the following reasons: rapid quenched specimens exhibited quench cracks which prevented valid mechanical testing, the initial quenched state can be characterized and the effect of the $DO_3 \rightarrow L1_0$ transition of the binary phase on the aging behavior could be investigated.

II. EXPERIMENTAL PROCEDURES

The alloy $Cu_{2.5}Mn_{0.5}Al$ was prepared by melting high purity elements; 99.999%Cu, 99.9%Mn and 99.999%Al in an induction furnace under a helium atmosphere and was chill cast into a copper mold. The composition of the alloy, in weight percent was; 47.3/Cu; 13.1/Mn; 12.6/Al. Chemical analysis verified to within ±1% the given composition. The ingot was then placed in a stainless steel envelope under an atmosphere of argon, homogenized at 850°C for 72 hr and oil quenched in order to avoid quenching cracks. The ingot was heated to 890°C (melting point is 910°C) and was air cooled after being rolled. The above homogenization was repeated again after rolling.

After cutting and machining the various experimental specimens from the ingot they were homogenized under an atmosphere of argon at 850°C for 20 min and oil quenched. After these heat treatments, specimens had grain diameters of about 1-6 mm. The specimens were then aged for various times in the temperature range 225°C to 325°C. The aging treatments were carried out in oil baths at temperatures below 250°C and in a salt bath (50% potassium nitrate, 50% sodium nitrate) above 250°C. These aging treatments were done for all six different experimental specimens,

1. Tensile test specimens,
2. Compression test specimens,
3. Quench rate specimens,
4. Vicker's hardness specimens,
5. Curie temperature measurement specimens,
6. Electron microscopy specimens.

Tensile test. The specimens for tensile tests were cut from the ingot, with the dimensions given in Fig. 3, then were aged at 290°C for 20, 200, 5500, 8500 min.

Compression test. The compression test specimens of dimensions 0.1×0.1×0.3 in. were cut from the ingot. Cylindrical grips were used to hold the specimens for compression and molybdenum sulfate was used as a lubricant. An Instron testing machine was used for both compression and tensile testing. The experiments were all performed at room temperature, at a constant cross head speed of 0.02 in./min.

Quench rate measurements. 10^{-3} $in.^3$ cubes were cut from the homogenized ingot, then connected to a thermocouple. They were heated up to 800°C and quenched and the cooling rates were simultaneously monitored on an x-y recorder with a chart drive speed of 2.5 cm/min accuracy was limited to 1 sec by the line width of the needle print out derive. The specimens were cooled in four different media with the following cooling rates.

Furnace cooled	$R \sim 3$ C°/sec
Air cooled	$3 < R < 300$ °C/sec
Oil quenched	$45 < R < 150$ C°/sec
Ice brine quenched	$R \sim 300$ C°/sec

R = rate of cooling.

Vickers hardness measurements. Vickers hardness was determined for three sets of specimens which were aged at 225°C, 275°C and 325°C for 2, 10, 20, 50, 180, 400, 1000, 3000, 6000, 10,000 min. A Miniload hardness tester was used with a 1000 gm weight for producing the test load, a minimum of six measurements was made on each specimen upon

surfaces polished with one micron diamond paste. The mean values and the standard deviation of different measurements for each specimen was calculated to obtain the hardness curve. The Vickers hardness of specimens after different quench rates were also measured using the same procedure.

Curie temperature measurements. The Curie temperatures of the as quenched specimens were measured using an apparatus developed at the Lawrence Livermore Laboratory for the study of high temperature magnetic phase changes. This apparatus is essentially a transformer in which the specimen is the core between the primary and secondary coils. The apparatus is made of boron nitride, quartz tubing and platinum wire. An x-y recorder was used to measure changes in induced voltage of the secondary coil as a function of temperature. Heating and cooling cycles were run for each specimen, and the average value of the measured temperatures was taken as the Curie temperature. The specimens used for these measurements were 0.5 cm × 0.5 cm × 2.5 cm. A nickel specimen was used as a standard, from which the accuracy of the measurements could be estimated.

Electron microscopy. The 0.5 mm thick foils obtained as described above were heat-treated along with the other specimens. Foils for electron microscopy were prepared after the heat-treatments by spark cutting to 2.3 mm dia discs, followed by thinning in an automatic jet polisher using an electrolytic solution of 400 ml acetic acid, 20 ml water, 75 gr chromic oxide. All observations were made in a Siemens IA electron microscope equipped with a double-tilt specimen stage.

The wavelengths of decomposition (λ) were either measured directly from the observed modulations in electron micrographs, or more accurately

by calculation from the spacing of satellites which occur along ⟨100⟩ in diffraction patterns. Thus all micrographs were taken in the ⟨110⟩ or ⟨100⟩ orientations with a strong 400 reflection operating. For specimens with λ ⟨ 150Å the side-band spacings on 400 reflections were used to calculate λ from the formula[11] for cubic phases

$$\lambda = \frac{h \tan\theta}{(h^2 + k^2 + \ell^2)\ \sigma\theta}\ a_o$$

a_o = average lattice parameter of DO_3 and $L2_1$ phases.

Δr = distance from the 400 sideband to the 400 reflection on the plate

r = distance from the origin (000) to the 400 reflection on the plate

The difference in lattice parameters Δa

$$\Delta a = \Delta d \left(\sqrt{h^2 + k^2 + \ell^2}\right)$$

was calculated from the "splitting" of spots $\{hk\ell\}$ in diffraction patterns, having ⟨110⟩ or ⟨100⟩ orientation so as to resolve the two spots. Usually the 800 reflection was excited which are spaced a distance ($\Delta d \cdot \lambda L$) on the plate.

X-ray measurements. All X-ray diffraction pictures were taken with 114.6 cm diameter Debye-Scherrer cameras; nickel filtered copper radiation was used. The 0.0021 in. diameter powder specimens were capsulated in the quartz tubes and were photographed in the camera.

III. RESULTS

A. The As Quenched Alloy

In order to correlate the difference in structure and properties of the alloy with different quenching rates, four sets of specimens were quenched in different media (ice quenched, oil quenched, air cooled, furnace cooled). The difference in microstructure of ice brine, oil quenched, air cooled and furnace cooled samples is shown in Figs. 4a, b, c and d respectively. The corresponding diffraction patterns are shown in Figs. 5a, b, c and d. These figures indicate that both ordering and spinodal decomposition (to a Cu_3Al rich phase and a Cu_2MnAl rich phase) occurred during the quench. The fundamental spots (400), (220) etc in Fig. 5 are associated with the bcc cell on which the structure is based. The superlattice spots (200), (311), (111) etc are associated with the ordering to DO_3 and $L2_1$ type structures, and the side bands which are clearly resolved in Fig. 5b are due to the formation of the periodic structure e.g., resolved in Fig. 4b. The side band spacing is inversly proportional to the wavelength. Figures 4a and b show the "tweed" contrast.[10] In the diffraction pattern of Fig. 5a diffuse scattering along the ⟨110⟩ direction at 45° to the side bands is observed and which do not have maxima as in Fig. 5b. This suggests that such diffuse streaks may be due to elastic strains arising from the presence of a dense array of small coherent precipitates, which formed during the quench. Figure 4b shows that oil quenching has also produced a "tweed" texture, and the diffraction pattern (Fig. 5b) reveals the presence of discrete precipitate spots and sharper side bands. In diffraction patterns from air cooled specimens (Fig. 5c) the side band spacing is decreased and after furnace

cooling (Fig. 5d) they are very small so that the wavelengths were measured from bright field micrographs. The presence of the extra spots resolved in Figs. 5b, c and d diffraction patterns is believed to be due to the presence of the Ll_0 structure. The direct evidence for long range order is obtained by imaging so as to show antiphase domain boundary contrast (see Fig. 6).

The hardness of specimens quenched from 800°C, with four different rates is given in Fig. 7, which shows that the hardness decreased with increasing quenching rate whereas wavelength is increasing too, which is unusual. The wavelengths of the quenched specimens have been measured and the results are as follows:

Iced brine quenched	22±3Å
Oil quenched	35Å
Air quenched	80Å
Furnaced cooled	250Å

The results for the iced brine quenched specimens lacks precision, because the satellites in the diffraction patterns were diffuse. The difference in lattice parameter of the two decomposed phases could not be measured in quenched samples because it was not possible to resolve any separation of spots in the diffraction patterns. This means that if the resolving power of the eye with the eye pieces be oil mm the Δa_{min} which can be detected must be:

$$\frac{a_1 - a_1}{a_1} = \frac{\frac{\lambda L \sqrt{h^2 + k^2 + \ell^2}}{r_1} - \frac{\lambda L \sqrt{h^2 + k^2 + \ell^2}}{r_2}}{r_1} = \frac{r_2 - r_1}{r_2} = \frac{\Delta r}{r_2}$$

$\frac{\Delta a}{a_1} = \frac{\Delta r}{r_2}$ if Δr = 0.1 mm and $r_2 \sim 14.3$ mm $\frac{\Delta a}{a}$ = 0.07 resolveable.

As it was expected the antiphase domain size was increased with the decrease in quench rate, but it's size was two large in comparison with the wavelength and the Ll_0 particles which were not resolveable. After slow quench the size of antiphase domain was >0.5 μ.

Based on the above data, the results of quenching can be categorized as follows:

1. Increasing the quench rates produces a decrease in Vickers hardness and smaller wavelengths. The structure resulting from rapid quenching consists probably of a two phase mixture of the binary-rich DO_3 and ternary-rich $L2_1$ phases.

2. Slower rates of quenching produces higher Vickers hardness readings and larger wavelengths. The structure of the ternary phase is again $L2_1$, but the binary phase itself may be decomposed (at least partially) to the Ll_0 structure. These results clearly show that there is no "classical" inverse wavelength dependence on the hardness.[1,2]

B. Morphology and Structure of Aged Alloys

The oil quenched specimens were chosen for subsequent aging treatments based on the following reasons. 1) Specimens quenched rapidly in iced brine exhibited quench cracks which prevented valid mechanical testing. 2) The initial quenched state can be characterized and the effect of the $DO_3 \rightarrow Ll_0$ transition of the binary phase on the aging behavior could be investigated. Thus oil quenched specimens were aged at 225°C, 275°C, and 325°C for times between 2 min up to 10 min. The micrographs corresponding to these treatments are shown in Figs. 8, 9 and 10. Figure 6

shows the APB contrast due to long range order, and the domain size grows from about 0.5 μ after quenching to greater than 1μ upon aging. Figure 8 is taken under contrast conditions to show the two phase modulated conditions and shows the early stages of coarsening, when the two principal phases are still coherent. Continued aging causes further coarsening (Fig. 9) and loss of coherency as evidence by the presence of the interphase dislocations (Fig. 10). The formation of the latter is discussed elsewhere.[12] The Cu_2MnAl phase which has the $L2_1$ ordered structure showed no evidence for decomposition as was found in the Cu_3Al rich phase. With further aging, however, other precipitation reactions occur[7,8] and these will be discussed later.

During the early stages of coarsening since it was not possible to resolve the $L1_0$ particles by dark field imaging, their presence was dedected only by the detection of $L1_0$ reflections in diffraction patterns. However, it is not possible to estimate any changes in volume fraction of these particles from diffraction studies alone because of the complexities of intensities in electron diffraction. By further aging the development of the $L1_0$ tetragonal structure is clearly resolved in diffraction patterns (Fig. 11) and by dark field imaging of these $L1_0$ reflections (see Fig. 12). Figure 12 shows two variants of the $L1_0$ phase, using the $L1_0(201)_1$ and $L1_0(201)_2$ reflections shown in Fig. 12b and c. A comparison of the dark field micrographs (Fig. 12b and c) with the bright field micrograph (Fig. 12a) shows that the binary phase mostly contains $L1_0$ "particles". Dark field images of Fig. 13a and b show the $L1_0$ particles during later stages of aging at 275°C. The dark field micrograph of Fig. 13a and b obtained by using $L1_0(310)$ reflection in

Fig. 14, clearly shows that as the aging time was increased, the volume fraction of the $L1_0$ phase was decreased. Quantitative data on this variation is very difficult to obtain because of resolution limitations. A rough measurement of the ratio of the $L1_0$ phase to the binary phase between 300 min to 3000 min aging at 275°C shows a decrease by about a factor of 3. These data were obtained by carrying out linear dimensional analysis directly from bright and dark field micrographs.

When coherency was lost, $L1_0$ particles exhibited a distorted structure similar to the martensite plates in CuAl alloy.[13] This is shown in Fig. 15 for specimen aged at 325°C for 3000 min using the spot marked M in diffraction pattern 14, Bouchard and Thomas[7] also observed these two characteristic features of the transformations in the binary rich (Cu_3Al) phase. The Cu_3Al rich phase also transforms to the γ-type structure, with the composition close to Cu_9Al_4.[8] Precipitation of the γ-phase inside the grain is shown in Fig. 16. The identification of the γ-phase is shown in the diffraction pattern of Fig. 17. Figure 18 shows the coarsening of γ particles and also the change in volume fraction of the binary and ternary phases. The volume fraction of the binary phase has considerably increased after aging for 3000 min at 325°C, and the volume fraction of the two phases (Cu_3Al rich and Cu_2MnAl rich) has become close to 2:1, instead of 1:1 as expected from Fig. 1.

C. Measurements

1. Tensile and Compression Tests

The oil quenched specimens of the tensile tests were aged at 290°C for different aging times. They were so brittle that they fractured before reaching the plastic region in the stress-strain curve.

Occasionally the specimens fractured outside the gage length, which was the result of propagation of micro cracks formed during the quenching or rolling. The stress strain curves obtained by these experiments are shown in Fig. 19. As indicated by these curves, there is no change in initial slope as the aging time increases which indicates that aging did not improve the ductility. Some of the curves are not smooth because the specimens slipped in the grips during the experiment. The compresion test also was not successful for measurements of yield stress, they fractured in elastic region and never were plastic. In the foils prepared from the fractured areas of deformed specimens, dislocations were not resolved at all or in some cases only a very few were observed as shown in Fig. 20 for the compression specimen.

2. Vickers Hardness

The results of Vickers hardness measurements, for oil quenched specimens which were aged at 225°C, 275°C and 325°C, four times between 2 min up to 10,000 min, are summarized in the graph shown in Fig. 21. After aging at 225°C the hardness increased rapidly and stayed constant after 180 min. The hardness of specimens aged at 275°C first increased and reached a maximum around 20 min aging, and after 50 min decreased until 1000 min. Further aging from 1000 to 10,000 min did not change the hardness. The total changes of VHN was small ~5% at 275°C aging. Specimens aged at 325°C had a slight decrease in hardness, and after 180 min aging the hardness increased to a peak at 3000 min. Beyond 3000 min another decrease was observed.

3. Wavelength

In spinodally decomposed alloys, as the aging time is increased, the wavelength of the modulations increases. In order to find out if there is a correlation between hardness and wavelength, the latter (λ) was measured for different times and temperatures. The results of these measurements are summarized in the log scale plot of λ vs t (time) in Fig. 22. As the aging temperature increases the slope of the curves increase as shown in Fig. 22. The relation between log λ and log t is linear in the early stages of coarsening and can be represented by $\lambda = kt^n$ (n indicates the slope of the log-log plot). The values of n were 0.11, 0.3 and 0.38 at 225°C, 275°C and 325°C respectively. For longer aging times the slope of the curves change and the relationship between log λ and log t is no longer linear. In the later stages of coarsening, regions with higher wavelengths ($\lambda \approx 1400$Å) were observed to be separated by regions having smaller wavelength (200Å). This is shown in Fig. 23. The coherency is lost after $\lambda \approx 2000$Å. The curves in Fig. 24 show that there is no linear dependence between Vicker's hardness and wavelength.

4. Curie Temperature

For magnetic materials, changes in composition can be detected by changes in Curie temperature. For this measurement, specimens were heated up to 400°C and then furnace cooled. Heating and cooling curves were recorded, and from the average of their slopes, the Curie temperatures θ_C were measured. Repeating this experiment with the same specimen gave lower Curie temperatures for the second and the third run. The Curie temperatures of Cu_2MnAl and $Cu_{2.5}Mn_{0.5}Al$ alloys were measured, and the results were:

θ_C (Cu_2MnAl) = 320±10

θ_C ($Cu_{2,5}Mn_{0.5}Al$) = 314±10

Bonzurt[14] gives the Curie temperature of Cu_2MnAl:

aged at 110°C θ_C = 450°C

quenched from 850°C θ_C = 325°C

other references[15,16] give about the same data given above for the aged material.

The Curie temperature and the miscibility gap temperature (350°C) are very close for $Cu_{2,5}Mn_{0.5}Al$ alloy and the specimens could not be aged above the miscibility gap temperature. This together with the fact that the difference in Curie temperatures for Cu_2MnAl and $Cu_{2.5}Mn_{0.5}Al$ was very small and the accuracy of the readings was only ±10°C indicated that any changes in composition could not be resolved by the Curie temperature measurements. Therefore, the difference in lattice parameters Δa, which has a linear relationship with θ_C[17] was used for this analysis.

5. Difference in Lattice Parameters Δa

Figures 25 and 26 show changes in lattice parameter a of the two decomposed phases as a function of time for oil quenched specimens aged at 275°C and 325°C. These values were measured from (100) and (110) diffraction patterns using (008) spots. However, it was not possible to resolve the $L1_0$ reflection separately from the DO_3 reflections. Therefore, the results are given for $L2_1$ and DO_3 structures. During the aging at 275°C, there was a slight increase in lattice parameters of both phases (Cu_3Al and Cu_2MnAl), and by aging at 325°C the two lattice parameters

first increased but stayed constant after loss of coherency. These measurements could not be accurate for the binary phase lattice parameter calculation since the binary phase reflections had streaks due to the presence of the $L1_0$ phase. Therefore, the difference in lattice parameters (Δa) resulting from the above measurements is not reliable. The difference in lattice parameters (Δa) resulting from these measurements are summarized in Fig. 27 and there are no large changes in Δa after 180 min aging at 275°C, and 50 min aging at 325°C.

In order to minimize the errors involved in these measurements the ratio

$$\frac{\Delta a}{a_1} \, , \left(\frac{\Delta a}{a_1} = \frac{\Delta g}{g_2}\right)$$

was calculated.

$$a^\circ = \frac{\lambda L \sqrt{h^2 + k^2 + \ell^2}}{r}$$

$$a_1^\circ = \frac{\lambda L \sqrt{h^2 + k^2 + \ell^2}}{r_1}$$

$$a_2^\circ = \frac{\lambda L \sqrt{h^2 + k^2 + \ell^2}}{r_2}$$

$$\Delta a = a_1^\circ - a_2^\circ = \frac{\lambda L \sqrt{h^2 + k^2 + \ell^2}}{r_1} - \frac{\lambda L \sqrt{h^2 + k^2 + \ell^2}}{r_2}$$

$$\Delta a = \frac{r_2 \lambda L \sqrt{h^2 + k^2 + \ell^2} - r_1 \lambda L \sqrt{h^2 + k^2 + \ell^2}}{r_1 r_2} =$$

$$\frac{(r_2 - r_1)\, \lambda L \sqrt{h^2 + k^2 + \ell^2}}{r_1 r_2}$$

$$\frac{\Delta a}{a_1^\circ} = \frac{r_2 - r_1}{r_2} = \frac{\Delta r}{r_2}$$

$$\frac{\Delta a}{a_1^\circ} = \frac{\Delta r}{r_2}$$

Δa = difference in lattice parameters

a_1 = lattice parameters of the ternary phase at each aging conditions

Δg = difference in magnitude of reciprocal lattice vector of the two phases

g_2 = magnitude of reciprocal lattice vector of binary phase

$\frac{\Delta a}{a_1}$ = strain

The changes of strain vs time also appears to exhibit the same behavior as the $\Delta a, t$ curve. Figure 28 shows the $\frac{\Delta a}{a}$, Vickers hardness and wavelength vs aging time for 275°C aging temperature.

X-ray data. The results of lattice parameter measurements by X-ray diffraction for specimens aged at 275°C are shown in Fig. 29. It shows that the lattice parameter of the ternary phase was increased while that of the binary phase was increased during the aging. The difference in lattice parameters Δa had increased during the aging at 275°C as is also shown in Fig. 29. Variations of wavelength, Δa measured from X-ray diffraction and Vickers hardness vs aging time for specimens aged at 275°C is shown in Fig. 30.

D. Summary of Results

1. During rapid quenching, the alloy decomposes to a modulated mixture of DO_3 (binary rich) and $L2_1$ (ternary rich) structures apparently by the spinodal reaction. The binary rich phase further decomposes to an Ll_0 phase during slow quenching.
2. Decreasing quench rates produced an increase in Vickers hardness and larger modulation wavelengths.
3. As it was expected the antiphase domain size was increased with the decrease in quench rate but it's size was too large in comparison with the wavelength and the Ll_0 particles which were not resolveable.
4. Specimens aged at 325°C coarsened rapidly and were observed to lose coherency after 1000 min. At 275°C, the rate of coarsening was considerably less, with loss of coherency occurring after 10,000 min aging. Aging at 225°C produced only a slightly coarsened structure after 12,000 min aging.
5. During the early stages of coarsening the binary phase appears to consist entirely of the Ll_0 structure. After further aging the Ll_0 structure transforms to DO_3, and the volume fraction of Ll_0 thus decreased during the later stages of aging. Specimens aged at 325°C exhibited the γ phase precipitation in addition to a tweed texture within the binary phase upon coarsening.
6. The volume fraction of the binary rich phase was found to increase during aging at 325°C.
7. Specimens aged up to 400 min at 225°C showed an increase in VHN after which the value leveled off at 460 VHN. A maximum in VHN (445) was

found in specimens aged at 275°C between 20 and 180 min. Longer aging resulted in a decrease and eventual leveling off of VHN at 430. A decrease in VHN during aging at 325°C resulted in a minimum (390) at 20 min followed by an increase to a maximum (415) at 3000 min.

8. Smaller values of VHN were observed to coincide with the presence of the DO_3 structure in the binary rich phase.

9. The relationship between log λ and log t was linear during the early stages of aging as expected for coarsening and could be represented by $\lambda = kt^n$. However, this relation became non-linear at the later stages of aging. Coherency was lost at $\lambda \approx 2000$Å, and for $\lambda > 400$Å the density of $L1_0$ particles decreased. Also the Vickers hardness was found to be independent of any variations in wavelength. (In as quenched specimens, VHN decreased with decreasing λ but this effect is due primarily to $L1_0$ not λ.)

10. In contrast to electron diffraction measurements, the X-ray measurements showed that during aging the lattice parameter of the ternary phase increased while that of the binary phase reduced, therefore, the difference in lattice parameter Δa increased.

IV. DISCUSSION

A. Discussion of the Metallography of Aging

1. As Quenched

The presence of side bands in Figs. 5a and b reveals that both the ice quenched and the oil quenched specimens have already spinodally decomposed, but the wavelengths of the ice quenched samples are ~12Å smaller than those of the oil quenched ones. Since, at higher temperatures, the DO_3 structure in Cu_3Al rich phase is the stable phase, then by rapid quenching the binary phase is expected to explain the structure of the high temperature stable phase. Alternatively a slower quench results in the appearance of the $L1_0$ structure, the low temperature stable phase. Increasing the quench rate decreases the amount of $L1_0$ (see Figs. 5b, c and d), indicating that DO_3 is more stable at the solution temperature. However, on aging the $L1_0$ reverts to DO_3 structure. The lattice parameter for DO_3 and $L2_1$ structures were nearly the same, and their differences could not be resolved in the diffraction patterns.

2. $L1_0 \rightleftharpoons DO_3$ Transformation

At the early stages of coarsening, the structure of the binary phase is mostly that of $L1_0$. This becomes apparent by a rough comparison of the volume fractions of the binary phase and $L1_0$ particles after 275°C aging (see Fig. 12). In the intermediate stages of coarsening the volume fraction of the $L1_0$ phase in the binary phase decreases by about a factor of 3 between 300 to 3000 min aging the decrease of volume fraction of $L1_0$ is shown in Figs. 13a and b. By aging at temperatures above 275°C, the binary phase possesses mostly the DO_3 structure, with the relative absence of the $L1_0$ particles, until the

Ll_0 reflection in the diffraction patterns finally vanishes. This suggests the presence of another miscibility gap inside the spinodal for the Ll_0 phase, above which the Ll_0 phase is not stable.

3. Coarsening

The log-log plots of wavelengths vs aging time (Fig. 22) could best be presented by the relation $\lambda \propto Kt^n$ with the temperature dependent exponent n = 0.11, 0.30 and 0.38 for 225°C, 275°C and 325°C aging temperatures respectively.

Typical microstructures obtained at 275 and 325°C are shown in Figs. 8-10. For the symmetrical Cu-Ni-Fe alloy Butler[17] found that particle coarsening could be described by the rate law $\lambda \propto Kt^{1/3}$, which is consistent with the theories of diffusion controlled coarsening, in which large particles grow at the expense of small ones. But for the asymmetrical Cu-Ni-Fe alloys, Livak and Thomas[4] found $\lambda \propto Kt^{0.37}$. The exponent n = 1/3 was predicted by Lifshitz, Slyozov and Wayner[18] in their theory of coarsening. For the $Cu_{2.5}Mn_{0.5}Al$ alloy, Bouchard and Thomas[6] found values of n = 0.127, 0.172 and 0.216 at 200°C, 240°C and 300°C aging temperatures respectively. Because of the difference in the initial quench rate, the values n = 0.30 and 0.38 obtained in this research do not agree with results reported by Bouchard and Thomas, but they are close to the theoretical value n = 1/3. The n = 0.11 obtained for 225°C aging temperature does not support the theory of particle coarsening; however, the values of n are in agreement with the theoretical prediction of Cahn,[19] that the average wavelength gradually shifts toward larger wavelengths.

The variation of coarsening rate with temperature can be modified due to the transformations within Cu_3Al rich phase e.g., the influence of the $L1_0$ phase.

4. Correlation of Wavelength and $L1_0$ Phase

$L1_0$ particles are present in the as quenched state because of the slow quenching rate. As mentioned before (Section 1), after aging at low temperatures (225°C) the $L1_0$ phase has a very high density, which is related to the slower rate of coarsening. At higher aging temperatures (275°C and 325°C), the density of the $L1_0$ phase decreases. When the $L1_0$ structure is suppressed by iced brine quenching, the binary phase has a DO_3 structure. Subsequent decomposition occurs along the elastically soft ⟨100⟩ directions of the binary (DO_3) and ternary ($L2_1$) "matrix" structures. Slower quenching allows the $L1_0$ structure to emerge in the following orientation relationship with the ternary phase:

$$(010)_{L1_0} \parallel (001)_{L2_1}$$

$$[001]_{L1_0} \parallel [110]_{L2_1}$$

Decomposition in this case occurs at 45° to the ⟨100⟩ direction of the $L1_0$ phase. Hence the presence of $L1_0$ particles could act as a barrier opposing coarsening of the major (modulated) phases in the ⟨100⟩ direction of the matrix. From Fig. 11b

$$[001]_{L1_0} \parallel [220]_{L2_1}$$

$$[201]_{L1_0} \parallel [031]_{L2_1}$$

therefore, the growth in $\langle 001 \rangle_{L1_0}$ directions of the $L1_0$ phase will be in the $\langle 220 \rangle_{L2_1}$ directions of $L2_1$, and due to the two competitive directions for wavelength growth in $\langle 220 \rangle_{L2_1}$ and $\langle 040 \rangle_{L2_1}$ directions of the matrix, a component of strain is expected to be parallel to the $(031)_{L2_1}$ or $(201)_{L1_0}$ planes. This is verified by the observation of streaks along the $\langle 201 \rangle$ direction in selected area diffraction patterns (see Fig. 11). These streaks are stronger in the early stages of coarsening, when the binary phase has mostly the $L1_0$ structure. Nevertheless, as the aging process proceeds, the amount of $L1_0$ decreases by transforming to DO_3. Therefore, the DO_3 and $L2_1$ structures dominate the decomposition due to their large volume fractions, and wavelength growth in the $\langle 100 \rangle$ direction of the matrix is ultimately observed.

From the above discussion it is concluded that by aging at low temperature (225°C, especially after a slow quenching rate, the $L1_0$ phase is present from the beginning of the aging process and, therefore, a lower rate of growth is obtained. For higher aging temperatures the growth rate is closer to the value n = 1/3 because of the decreasing importance of the $L1_0$ phase.

The changes in the rate of growth in the later stages of aging (see Fig. 22), can be expressed in the form of $\lambda \propto Kt^n$. As is shown in Fig. 23, the wavelength can vary by more than one order of magnitude within one wavelength of the larger modulation. A similar result was obtained by Bouchard and Thomas[6] for states following the loss of coherency.

B. Correlations of Structure and Hardness

Age Hardening. Ice quenched samples had the smallest, and furnace quenched ones had the highest hardness number (VHN) (see Fig. 7), and it was realized that like wavelength, hardness also was very sensitive to the quenching rate.

Cahn[20] calculated that a dislocation can slip through an interparticle opening if $\sigma_a b > \frac{2\gamma}{L}$ where γ is the self energy of the dislocation ($\sim Gb^2$), and L is the separation between particles. Although a symmetrical spinodal structure is characterized by a continuous network of composition modulations, well developed morphologies can be assigned an effective interparticle spacing on the order of $\lambda/2$. By application of this approximation to the early stage of the coherent structures, the applied stress necessary for slip is given by $\sigma_a > \frac{4Gb}{\lambda}$ showing that the stress varies as (λ^{-1}).

Since for brittle materials, the flow stress can be experimentally expressed in terms of hardness, one expects that the hardness should also vary as $(\lambda)^{-1}$.[21] However, in this investigation the (inverse) proportionality of VH and λ for quenched specimens was not observed. On the contrary it was found that slow quenching which produced larger wavelength is associated with higher Vickers hardness. Therefore, the controlling parameter for dislocation motion in the as quenched alloy is not the wavelength of the binary and the ternary phase, but the increase in VHN of the slow quenched samples is due primarily to the change of structure within the binary rich phase (Cu_3Al).

The higher hardness of the slow quenched specimens correlated with the presence of the noncubic $L1_0$ structure of the binary rich phase. These $L1_0$ particles in the Cu_3Al rich phase increase the hardness by a dispersion hardening mechanism. Arunachalam[21] has indicated that formation of the tetragonal $L1_0$ CuAu alloy is accompanied by a doubling of its strength where the strengthening increase is attributed to a change in lattice symmetry. The tetragonal structure sets up substantial misfit stresses within the cubic matrix, which in turn exert an affective friction force on moving dislocations. A similar mechanism is expected to be operable within the present system due to the $\frac{c}{a}$ ($\neq 1$) ratio of the $L1_0$ structure of the Cu_3Al phase. In addition, the existence of six variants of the $L1_0$ structure, two of which are shown in Fig. 12, may contribute further to the strengthening, due to the complexity of the resulting stress fields, and their possible interaction.

Aged specimens exhibit a general age hardening behavior viz, the maximum hardness increases with decreasing aging temperature and as the aging temperature decreases, the time to attain maximum hardness increases (see Fig. 21). The hardness charges for specimens aged at 225°C, 275°C and 325°C can be divided into three major stages: first, an increase in hardness is observed during the early stages of coarsening; second, a reduction in hardness from its maximum value occurs simultaneously with a decrease in the volume fraction of the $L1_0$ structure; and finally, no hardness change is seen in the overaged specimens, as the amount of the $L1_0$ structure is reduced essentially to zero. The details of the aging response during these stages are described below.

At the onset of coarsening, the changes in hardness are shown from the microstructure of the binary phase to result from the $DO_3 \rightarrow L1_0$ transformation. Increasing hardness in this case is due to the increasing misfit stresses from the larger volume fraction of the $L1_0$ structure $\left(\frac{c}{a} \neq 1\right)$ as discussed in the dispersion hardening model presented above. Additional evidence for this mechanism is given by the correlation of maximum hardness with maximum volume fraction of the $L1_0$ structure of the binary phase, which is found in specimens aged at 225°C and 275°C (early stages).

The decrease in microhardness of specimens aged at 275°C can be correlated with two parameters: 1) Increase in wavelength of the binary and the ternary phases and 2) reduction in volume fraction of the $L1_0$ structure (Fig. 13) within the (Cu_3Al) rich phase. As was discussed earlier in this section, it was expected that the hardness would be inversely proportional to λ. However, this inverse proportionality was not observed at 225°C nor 325°C but only in specimens which overaged at 275°C (i.e., between 20 min and 1000 min), corresponding to wavelength growth from 200 Å to 400Å (Fig. 24). The inverse proportionality of hardness and λ in the intermediate stage of aging at 275°C is revealed by the negative slope of the hardness vs λ curve. But the rate of increase of λ is much greater than the rate of decrease of Vickers hardness, so if the increase in λ had contributed to the decrease of

hardness it would have decreased it in a much faster rate. Therefore, it is believed that the soltening at overaged stages to be mostly due to the $L1_0 \rightarrow DO_3$ transformation. As the amount of tetragonal misfit is reduced, the hardness also decreases. The reduction in hardness might also be explained on the basis of an Orowan model,[22] where the flow stress (τ), after Kelly[23] is given by:

$$\tau = \frac{Gb}{d}$$

for G = shear modulus and b = Burgers vectors of the slip dislocation assuming flow only in the Cu_3Al rich phase. The interparticle spacing (d) increases as the amount of the $L1_0$ structure decreases, resulting in a decreased flow stress. Finally, the lowest VHN values were found in specimens aged for short times at high temperatures (325°C, where the Cu_3Al rich phase had a nearly continuous DO_3 structure with no evidence of $L1_0$ particles.

After the loss of coherency an increase followed by a decrease in VHN was detected for over aged specimens at 325°C. These changes correspond with the precipitation of γ particles (Figs. 16-18), martensite plates in the over aged conditions (Fig. 15), and the change in the volume fraction of the binary and the ternary phase (Fig. 18).

The changes of difference in lattice parameters of the two (Cu_3Al-Cu_2MnAl) principal modulated phases (Δa) is another factor that can affect the strength of the alloy. Livak and Thomas,[4] by extending the

Mott and Nabarro[23] theory to two phase spinodals, found a direct proportionality between the yield stress and the difference in cubic lattice prarmeters of the two precipitating phases in Cu-Ni-Fe alloy. Mott and Nabarra proposed that because of the difference in atomic volume that exists between two coherent phases, there will be an internal stress field which will oppose dislocation motion. In a opinodal system this elastic strain field will have the same wavelength as the composition fluctuation. The theory predicts that the average internal stress is independent of particle size but is dependent on G (average shear modulus), ϵ (size factor between solute and solvent) and on f (volume fraction) via the relation $\sigma_i \sim 2G\epsilon f$, on the other hand, since $\epsilon \propto \sigma$ $\sigma = \frac{\Delta a}{a}$, the relation $\sigma_i \propto \frac{\Delta a}{a}$ is easily found by substituting the last two relations in the first equation for σ_i. It was, therefore, expected that the Vickers hardness of the $Cu_{2.5}Mn_{0.5}Al$ alloy would be dependent on the difference in lattice parameters. However, this dependency of microhardness and Δa could not be verified for as quenched specimens because the difference (Δa) could not be resolved in diffraction patterns.

The lattice mismatch between DO_3 and $L2_1$ phases for aged specimens were measured from electron diffraction patterns (Fig. 27) and X-ray diffraction method (Fig. 29). The electron diffraction patterns are taken from the part of specimens $\sim 2\times10^4\times2\times10^4\times10^2 = 4\times10^{10}$Å while the X-rays diffraction patterns is from a volume $\sim 10^{21}$Å which is 11 order of magnitude larger.

This comparison can explain the difference between the data calculated from electron diffraction patterns and X-ray diffraction patterns. Since the electron diffraction pattern are obtained over one or two particles, they measure particular differences rather than a statistical average of the difference in lattice parameters over large volumes. In order to have a good average data from electron diffraction patterns a very large number ($\sim 10^{11}$ times) of electron diffraction patterns should be measured to have the same statistical results as X-ray results.

From the theory discussed above it was expected that an increase in Δa (see Fig. 29), which results in an increase in strain, to be related to the increase of VHN but Fig. 30 shows that the change in Vickers hardness due to aging is not directly proportional to Δa. Consequently this theory does not appear to be applicable to this situation. However, this theory can be applied in the cases that the two decomposed phases are controlling the mechanical behavior, when the strain is caused by the difference in lattice parameters between the coherent binary and ternary phase, opposing the dislocation motion. In the present case it is believed that only the binary phase is responsible for hardness changes, and dislocation motion in the domains of the $L1_0$ phase control the hardness variations, it is expected that VH changes to be actually independent of Δa.

The strengthening in the early stages of decomposition (Cu_3Al and Cu_2MnAl) can be related to the size of the ordered domains (See Fig. 6). This point has been considered by Hanninketal[26] Cottrell[27]

and Stoloff and Davies in connection with Mg_3Cd.[28] They found that the peak hardness occurs at an antiphase domain size of ~60Å diameter in Mg_3Cd. However in the Cu-Mn-Al alloys, due to the slow quench the sizes of the antiphase domains are very large (0.5μ), by comparison to 60Å for Mg_3Cd. Also after short aging times they grow to larger than 1 μ dia (see Fig. 5). Thus the domain size effect in hardening is not appreciable.

V. SUMMARY

1. Upon quenching, the alloy spinodally decomposed to Cu_3Al and Cu_2MnAl compositions. While a rapid quench yielded the smallest wavelength and higher temperature stable structure (DO_3) in the binary rich phase, a slow quench resulted in larger wavelengths and the appearance of the $L1_0$ structure which is the low temperature stable phase.
2. The slower quenched specimens had a higher Vickers hardness than the rapidly quenched ones. This is associated with the presence of the $L1_0$ particles.
3. After the early stages of the aging the volume fraction of $L1_0$ particles in the binary phase decreased, due to transformation of $L1_0$ to DO_3. This suggests that a transition temperature of $L1_0$ phase inside the spinodal.
4. The rate of coarsening decreased with the presence of $L1_0$ particles. It is suggested that this is because of the competitive modulations in $\langle 100 \rangle$ directions of the matrix ($L2_1$, DO_3) and $L1_0$ phase which produced strain. The strain in $(201)_{L1_0}$ planes was detected by streaks in diffraction patterns in $[201]_{L1_0}$ directions.
5. For high aging temperatures the wavelength variations could be represented by $\lambda \propto kt^n$, and the values of n were close to the theoretical value for coarsening. But at low temperature aging, with higher volume fraction of $L1_0$, the value of n was smaller than the theoretical value.

6. Changes in Vickers hardness do not appear to be controlled by variations in wavelength in the as quenched specimens and the inverse proportionality of VHN and λ was observed only for specimens aged at 275°C from 20 min to 1000 min. Instead, the (small) changes in age hardening appear to depend mostly on $L1_0 \rightarrow DO_3$ transformations within the binary rich Cu_3Al phase.
7. Early stages of aging, with higher volume fraction of $L1_0$ particles in the binary rich phase which produced substantial misfit stresses within the cubic matrix, was observed to have the highest Vickers hardness. In the intermediate stages of aging since the size and the volume fraction of $L1_0$ particles were reducing, interparticles distances were increasing and the Vickers hardness was reduced. Finally, at the later stages of aging where binary phase had almost a continuous DO_3 structure, Vickers hardness had its smallest value.

ACKNOWLEDGEMENTS

The author wishes to express here deep appreciation to Professor Gareth Thomas for his interest, encouragement and valuable suggestions. She also wishes to thank R. Grownsky for his helpful discussions.

This research was supported by the U. S. Atomic Energy Commission through the Inorganic Materials Research Division of the Lawrence Berkeley Laboratory, Berkeley, California.

REFERENCES

1. J. W. Cahn, Acta Met. 2, 795 (1961).
2. J. W. Cahn, Acta Met. 10, 179 (1962).
3. M. Hillert, Acta Met. 9, 525 (1961).
4. R. Livak and G. Thomas, Acta Met. 19, 497 (1971).
5. M. Bouchard and G. Thomas, 29th Annual Proceedings of the Electron Microscopy Society of America, C. J. Arceneaux, ed., Boston, Mass., 1971.
6. M. Bouchard and G. Thomas, Modulated Structures and Coarsening in Order $(Cu\text{-}Mn)_3$ Al Alloys, UCRL-2294, 1973.
7. M. Bouchard and G. Thomas, Modulated Structures in $(Cu\text{-}Mn)_3$ Al Alloys II. Formation of An $L1_0$ Phase Within the Cu_3Al side phase, UCRL-2295.
8. M. Bouchard and G. Thomas, Modulated Structures in $(Cu\text{-}Mn)_3$ Al Alloys III. Formation of the γ phase, UCRL-2296, 1973.
9. M. Okada, M. S. thesis in progress.
10. G. Thomas, Modern Diffraction and Imaging Techniques in Materials Science, S. Amelinckx, R. Grevers, G. Remaut and I. VanLanduyt, eds. (North Holland Publishing Co., 1970), p. 131.
11. V. Daniel and H. Lipson, Proc. Roy. Soc. 182, 378 (1943).
12. M. Bouchard, R. J. Livak and G. Thomas, Surface Science 31; North Holland Publishing Co. 275 (1972).
13. P. R. Swann and H. Warlimont, Acta Met. 11, 511 (1963).
14. R. M. Bozorth, Ferromagnetism (Van Nostrand, New York, 1951).
15. C. Kittel, Introduction to Solid State Physics, (John Wiley, 1971), p. 461.
16. O. J. Keizoend, Phys. Soc. Japan 16, 1027 (1961).

17. E. P. Buttler, Structure and Properties of Spinodally Decomposed Cu-Ni-Fe Alloys, UCRL-18840, June 1969.

18. J. M. Lifshitz and V. V. Slyozov, J. Phys. Chem. Solids 19, 35 (1961).

19. J. W. Cahn, Acta Met. 14, 1685 (1966).

20. J. W. Cahn, Acta Met. 11, 1275 (1963).

21. V. S. Arunachalam, Ph. D. Thesis, University College of North Wales (1965).

22. E. Orowan, Symposium on Internal Stresses in Metals and Alloys, Inst. Metals (London), 451 (1948).

23. A. Kelly, Theories of Precipitation and Dispersion Hardening, in Electron Microscopy and Strength of Crystals, G. Thomas and J. Washburn, eds. (John Wiley, 1961).

24. D. Dew-Huges and W. D. Robertson, Acta Met. 8, 773 (1960).

25. N. F. Mott and F. R. N. Nabarra, Proc. Phys. Soc. 52, 86 (1940).

26. R. H. S. Hannink and M. J. Murry, Acta Met. 20, 123 (1972).

27. A. H. Cottrell, Relation of Properties to Microstructures (ASM Publication, 1954), p. 151.

28. N. S. Stoloff and R. G. Davies, Strengthening Methods in Crystals, A. Kelly and R. B. Nicholson, eds. (Elsevier, 1971), Chapter 4.

FIGURE CAPTIONS

Fig. 1. The ordering temperatures $T_c(B_2)$ and $T_c(DO_3\text{-}L2_1)$ and the miscibility gap of the $(Cu\text{-}Mn)_3$ Al alloys.

Fig. 2. The ordering reactions bcc$\rightarrow B_2 \rightarrow L2_1$ and isothermal decomposition to Cu_2MnAl and Cu_3Al, then generation of $L1_0$ structure from DO_3 structure.

Fig. 3. Dimension of tensile specimens.

Fig. 4. Bright field micrographs of specimen quenched in (a) iced brine, (b) oil, (c) air, and (d) furnace.

Fig. 5. (100) diffraction patterns of specimens quenched in: (a) iced brine, with no $L1_0$ precipitation reflection, (b) oil, with $L1_0$ reflection, sharper side bands and streaks in 011 direction, (c) air, intensity of $L1_0$ spots increased and (d) furnace, satellite (side band) spacing decreased.

Fig. 6. APB's in early stages of aging ($1\bar{1}0$ orientation). (a) Bright field micrograph of the specimen aged at 225°C for 10 min. (b) Bright field micrograph of the specimen aged at 275 for 2 min. (c) 111 dark field micrograph of the specimen aged at 325 for 30 sec. (d) 111 dark field micrograph of the specimen aged at 325 for 2 min. These show large APB because of slow quench (oil quenched).

Fig. 7. Log wavelength vs log quenching rate showing the increase of wavelength with decreasing quench rate, variation of hardness vs quenching rate and changes of wavelength with hardness.

Fig. 8. Bright field micrographs of specimens aged at 275°C from 20 to 180 min.

Fig. 9. Bright field micrographs of specimens aged at 275°C from 400 to 1000 min.

Fig. 10. Bright field micrographs of specimens aged at 325 from 50 to 3000 min.

Fig. 11. (a) (110) matrix ($L2_1$) diffraction pattern; one of the Ll_0 phase variants is indexed. (b) (001) matrix diffraction pattern; two variants of the Ll_0 phase are indexed. (c) (00) matrix diffraction pattern with streaks in Ll_0(201) direction.

Fig. 12. Bright field and dark fields of specimen aged at 275°C for 12000 min using (201), and $(201)_2$ reflection marked in Fig. 11b showing two of the Ll_0 varients. Particles are parallel to 220 directions. It also shows that binary phase has mostly the Ll_0 structure.

Fig. 13. Dark field micrographs of specimens aged at 275°C (a) for 400 min (b) for 3000 min, using Ll_0(310) reflection marked in Fig. 14 clearly shows that as the aging time was increased the volume fraction of the Ll_0 phase was decreased.

Fig. 14. $(110)_{L2_1}$ diffraction patterns of specimen aged 400 min at 275°C.

Fig. 15. Bright field and dark micrograph of specimen aged at 325°C for 6000 min. The reflection marked M in Fig. 14 was used to obtain the dark field. This reflection is believed to be a martensite reflection and in the micrograph the stacking faults in martensite are normal to the 220 direction.

Fig. 16. Bright field micrograph of specimen aged at 325°C for 20 min shows the precipitation of γ particles and formation of small angle boundary.

Fig. 17. (110) diffraction pattern. Extra reflections are indexed for γ particles. Specimen was aged 325°C for 20 min at 325°C.

Fig. 18. Bright field micrograph of specimen aged at 325°C for 3000 min, shows the precipitation of γ particle in the binary phase. Also shows the increase of volume fraction of the binary phase.

Fig. 19. Stress-strain curve of tensile test specimens ~0.1 as quenched, 2, 3, 4, 5 aged at 295°C for 20, 200, 5500, 8500 min respectively.

Fig. 20. Bright field micrograph of as quenched compression specimen obtained 0.1 in. far from the fracture surface. Shows the very small density of dislocations.

Fig. 21. Variation of Vicker's hardness vs log aging time for samples quenched in oil and aged at 225°C, 275°C and 325°C.

Fig. 22. Log wavelength vs log aging time, for samples quenched in oil and aged at 225°C-275°C and 325°C. The wavelengths of oil (35Å) and ice quenched samples (25Å) are also shown.

Fig. 23. Bright field micrograph of specimen aged at 325°C for 400 min. Area marked β shows the new small wavelength separating the particles with bigger wavelength.

Fig. 24. Variation of hardness vs log wavelength for specimens aged at 225°C, 275°C and 325°C from 20 to 7000 min.

Fig. 25. Changes of lattice parameters of DO_3 and $L2_1$ phases vs log aging time measured from electron diffraction patterns, for specimens aged at 275°C.

Fig. 26. Changes of lattice parameters of DO_3 and $L2_1$ phases vs log aging time, measured from electron diffraction patterns, for specimens aged at 325°C.

Fig. 27. Differences in lattice parameters of the two decomposed phases vs log aging times, measured from electron diffraction patterns, for specimens aged at 275°C and 325°C.

Fig. 28. Changes of wavelength, $\frac{\Delta a}{a_1}$ (from electron diffraction patterns) and Vicker's hardness vs log aging time.

Fig. 29. Changes of lattice parameters of DO_3 and $L2_1$ phases and their difference Δa, measured from X-ray diffractions, for specimens aged at 275°C.

Fig. 30. Changes of wavelength, Δa (from X-ray diffraction) and Vicker's hardness vs log aging time.

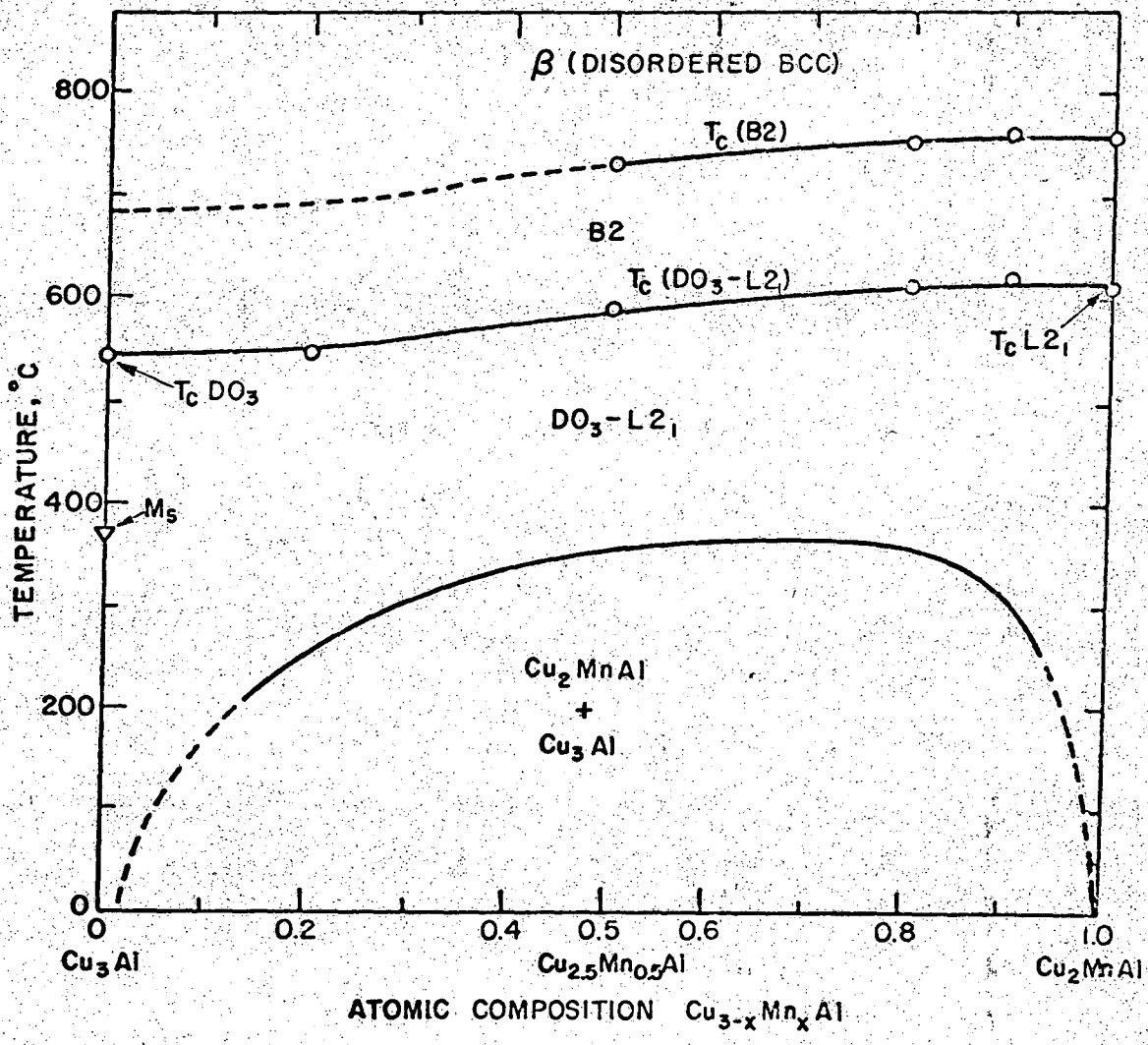
β (DISORDERED BCC)
800
T_c (B2)
B2
600
T_c (DO_3-$L2_1$)
T_c $L2_1$
T_c DO_3
DO_3-$L2_1$
TEMPERATURE, °C
400
M_s
Cu_2MnAl
+
Cu_3Al
200
0
0
0.2
0.4
0.5
0.6
0.8
1.0
Cu_3Al
$Cu_{2.5}Mn_{0.5}Al$
Cu_2MnAl
ATOMIC COMPOSITION $Cu_{3-x}Mn_xAl$
XBL7210-7116

Fig. 1

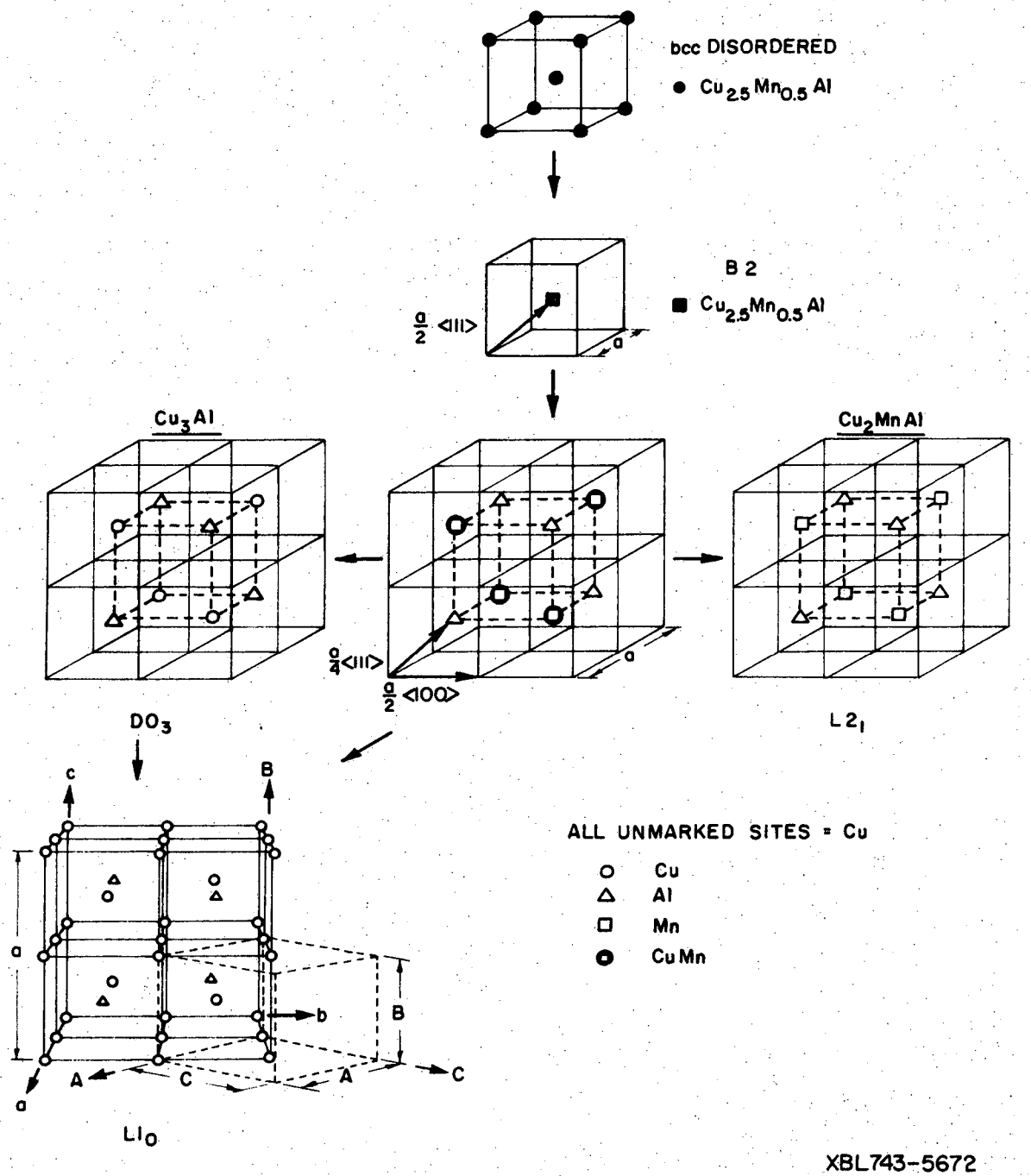
bcc DISORDERED
$Cu_{2.5}Mn_{0.5}Al$
B 2
$Cu_{2.5}Mn_{0.5}Al$
$\frac{a}{2}\langle 111\rangle$
a
Cu_3Al
Cu_2MnAl
$\frac{a}{4}\langle 111\rangle$
$\frac{a}{2}\langle 100\rangle$
DO_3
$L2_1$
c
B
a
b
B
A
C
A
C
a
LI_0
ALL UNMARKED SITES = Cu
Cu
Al
Mn
Cu Mn
XBL743-5672

Fig. 2

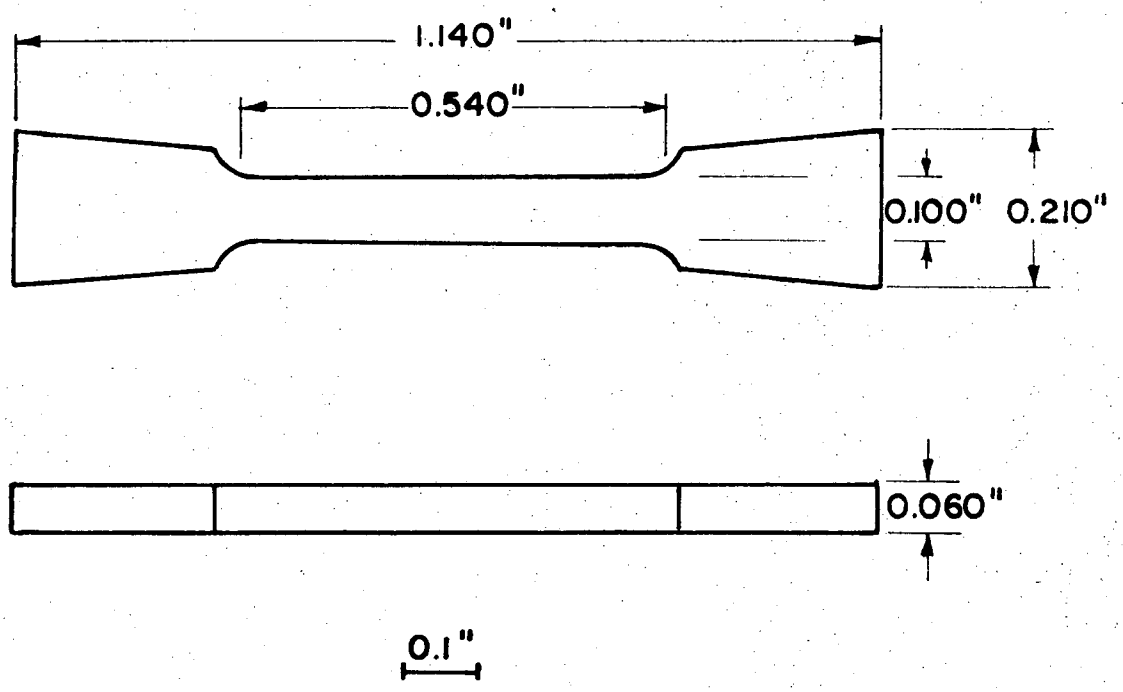

XBL 743-5667

Fig. 3

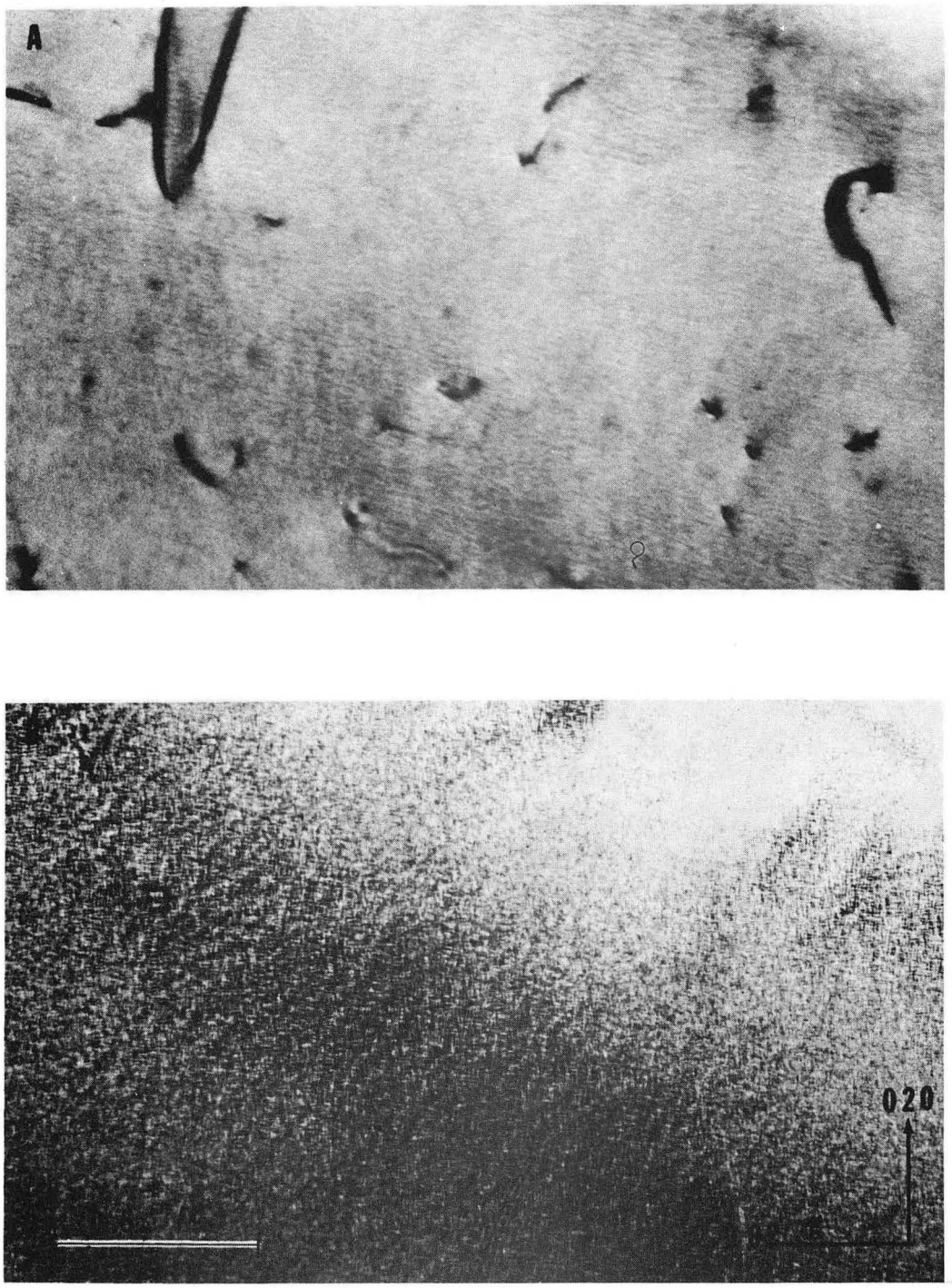

XBB 739-5600

Fig. 4

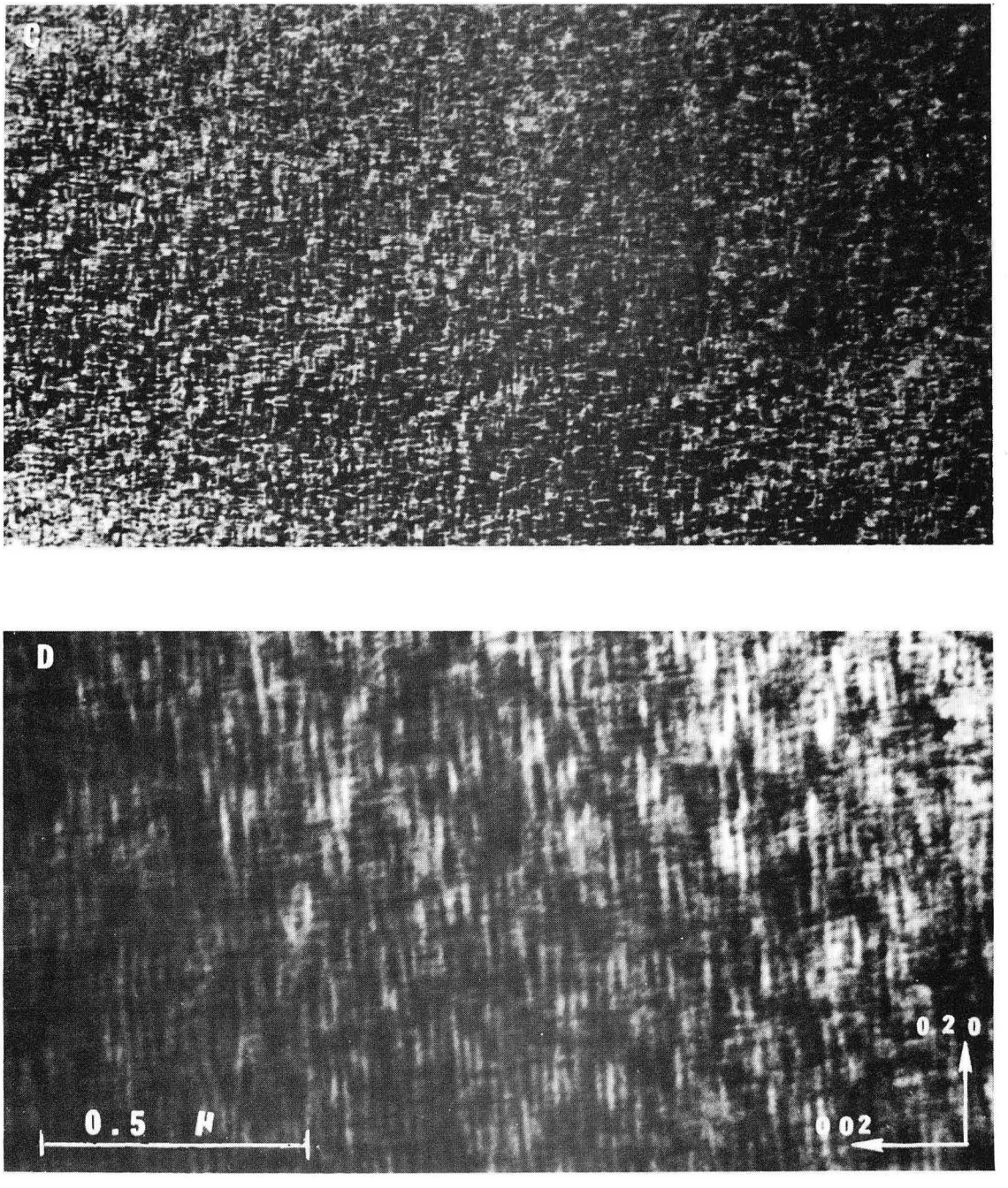

XBB 743-1866

Fig. 4 continued

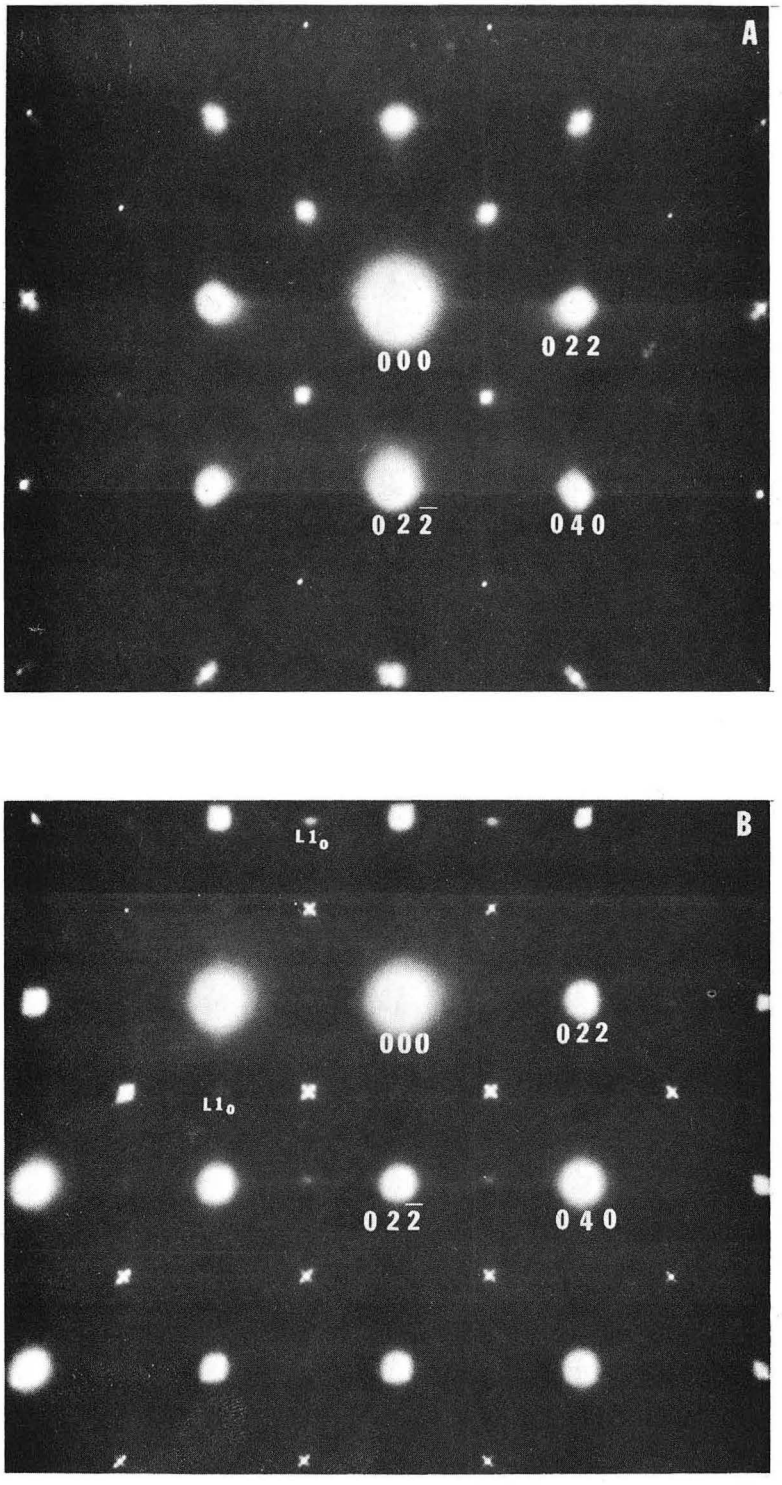

XBB 743-1864

Fig. 5

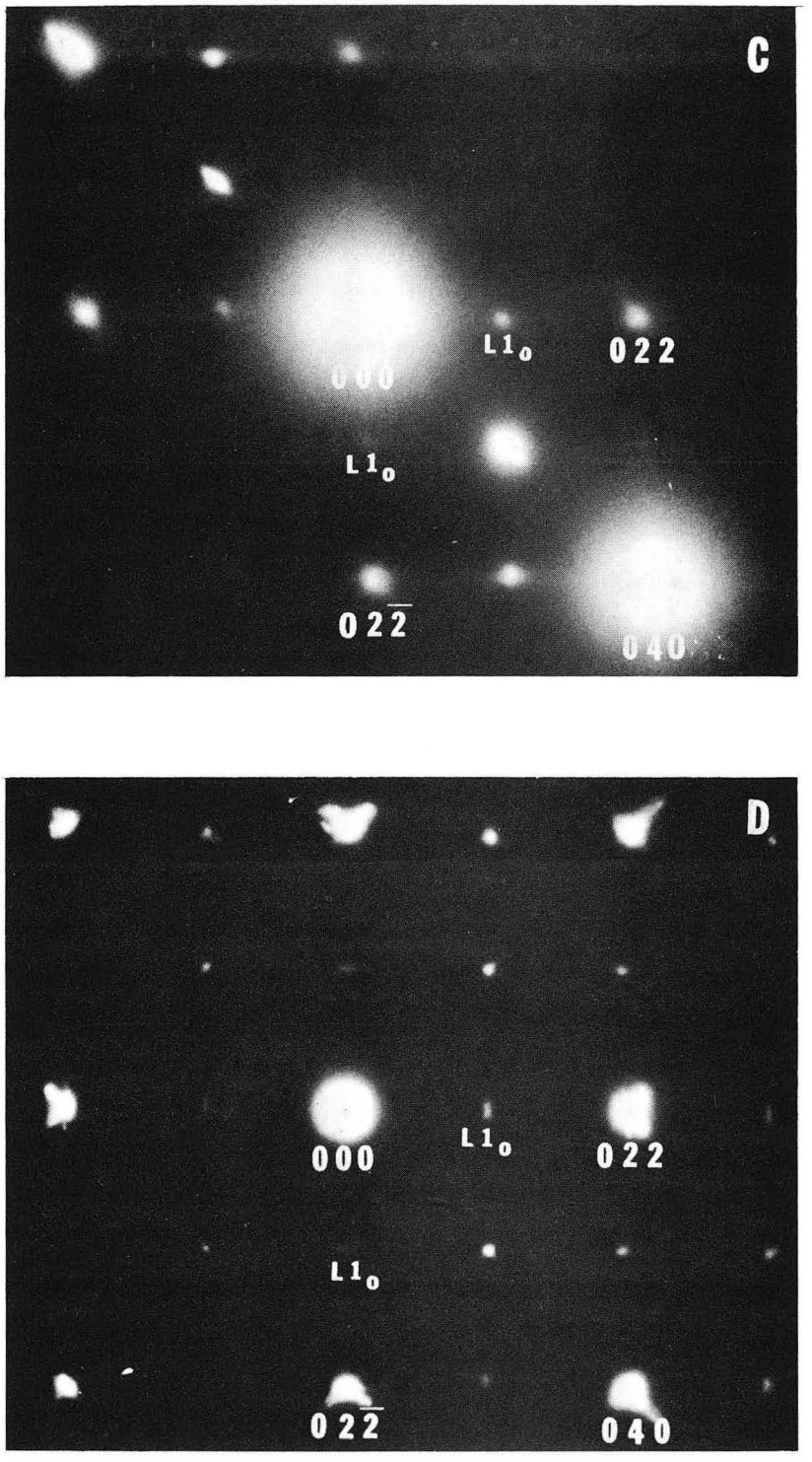

XBB 743-1865

Fig. 5 continued

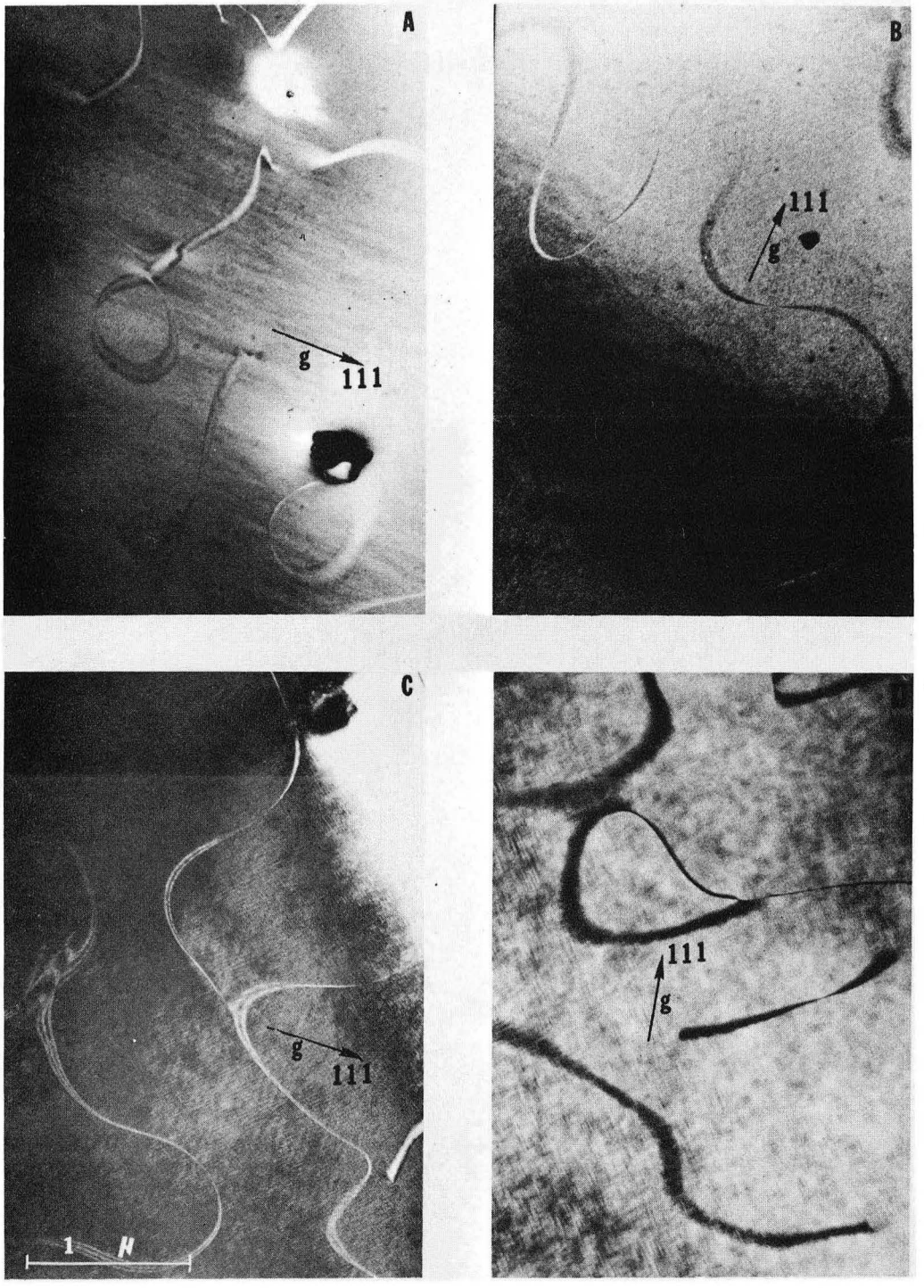

XBB 742-1238

Fig. 6

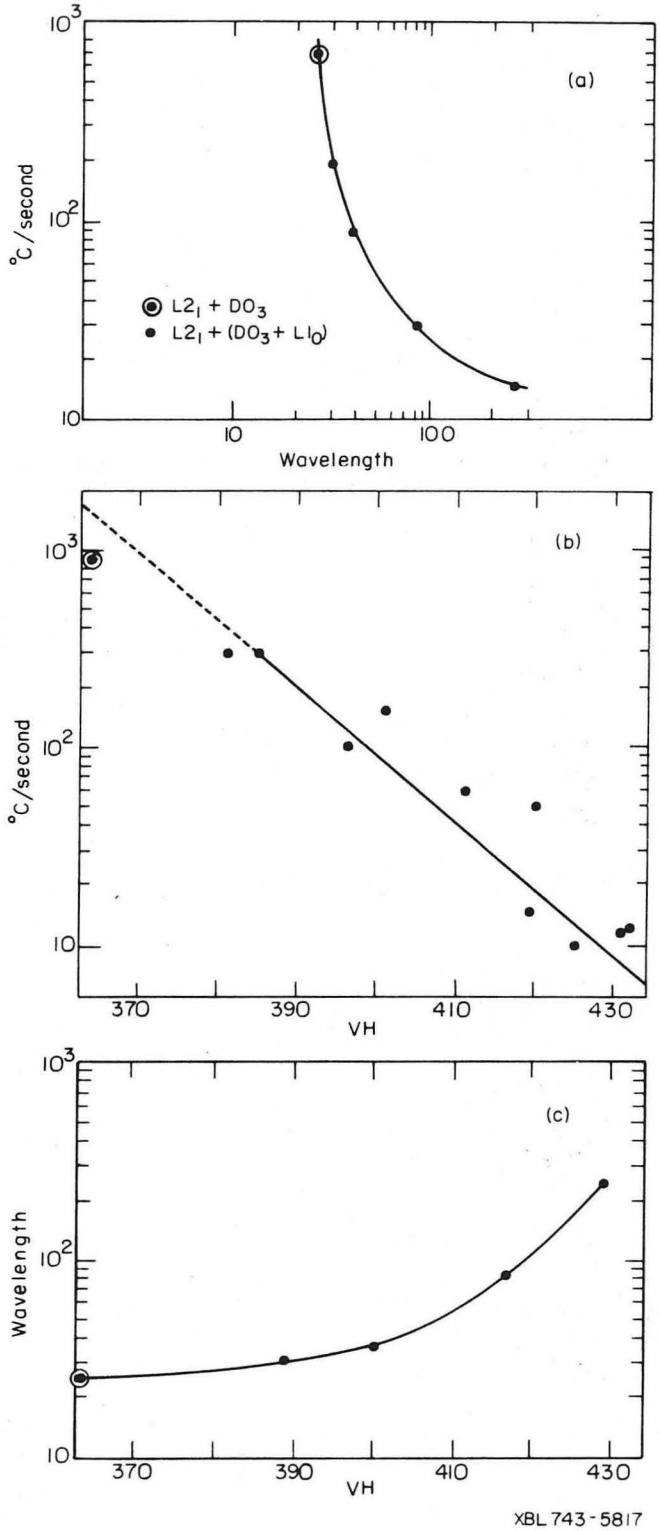
(a)
°C/second
Wavelength
L2₁ + DO₃
L2₁ + (DO₃ + L1₀)
(b)
°C/second
VH
(c)
Wavelength
VH
XBL 743-5817

Fig. 7

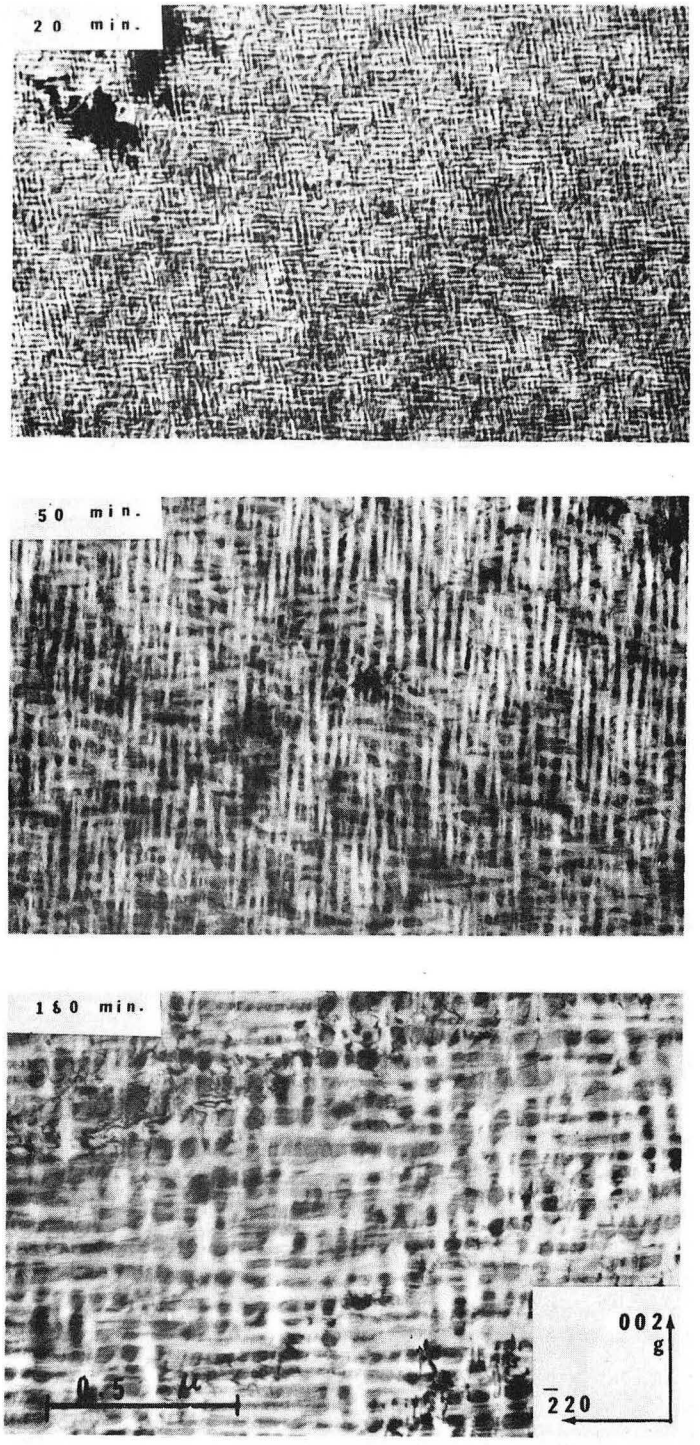

Fig. 8

XBB 742-1248

Fig. 9

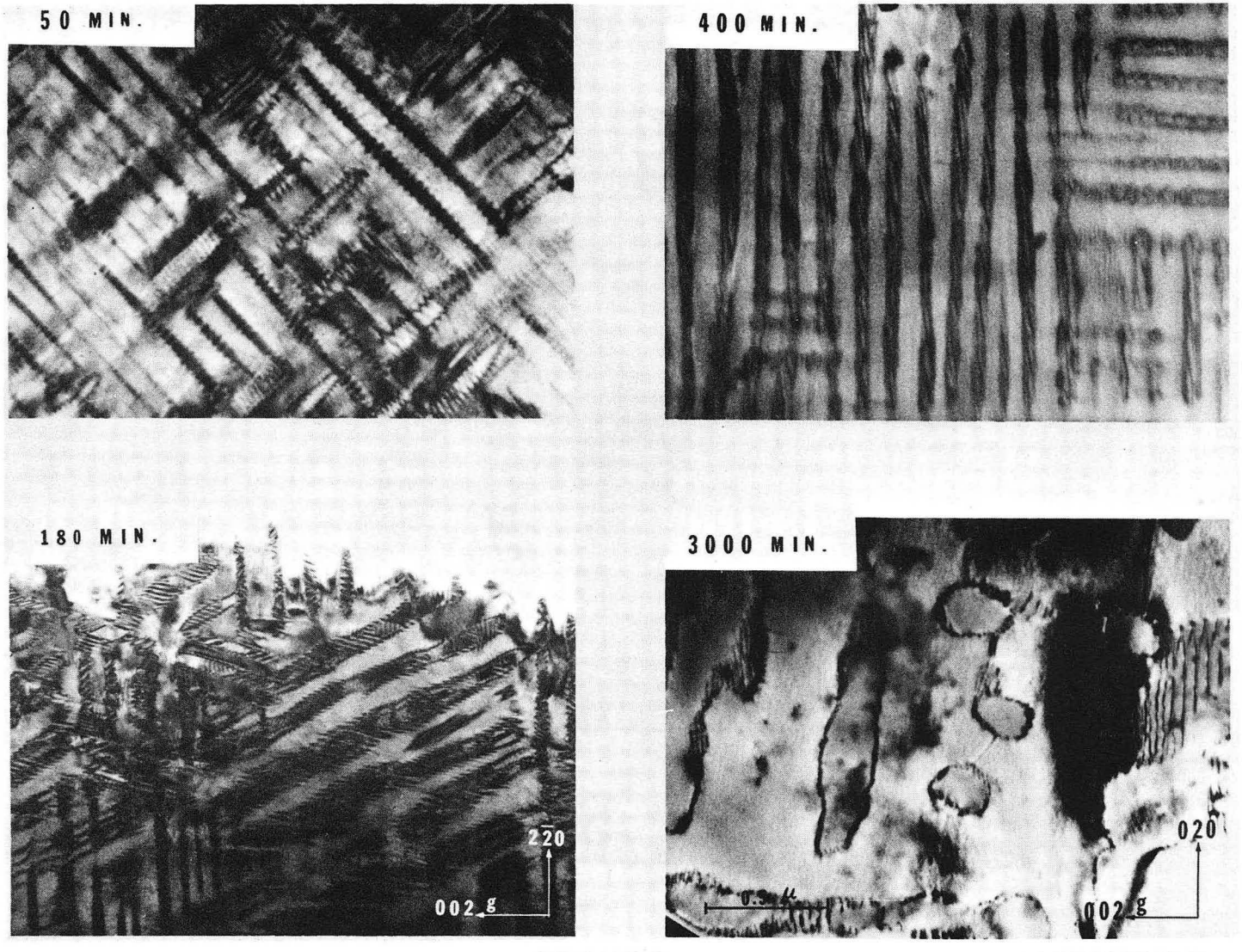
50 MIN.
400 MIN.
180 MIN.
3000 MIN.
220
002 g
020
002 g
0.5 μ
325 °C
XBB 742-1249

Fig. 10

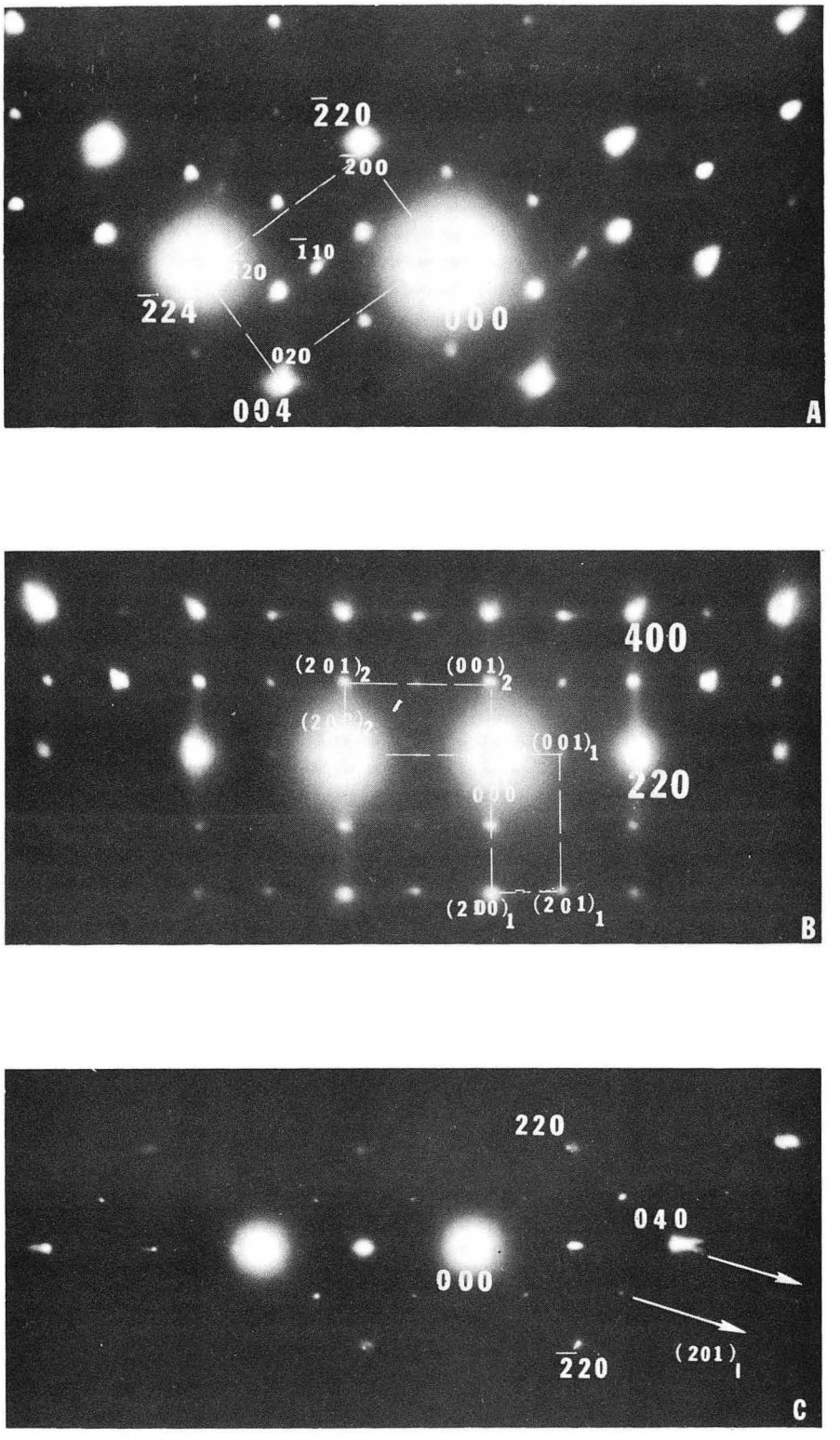

XBB 743-1863

Fig. 11

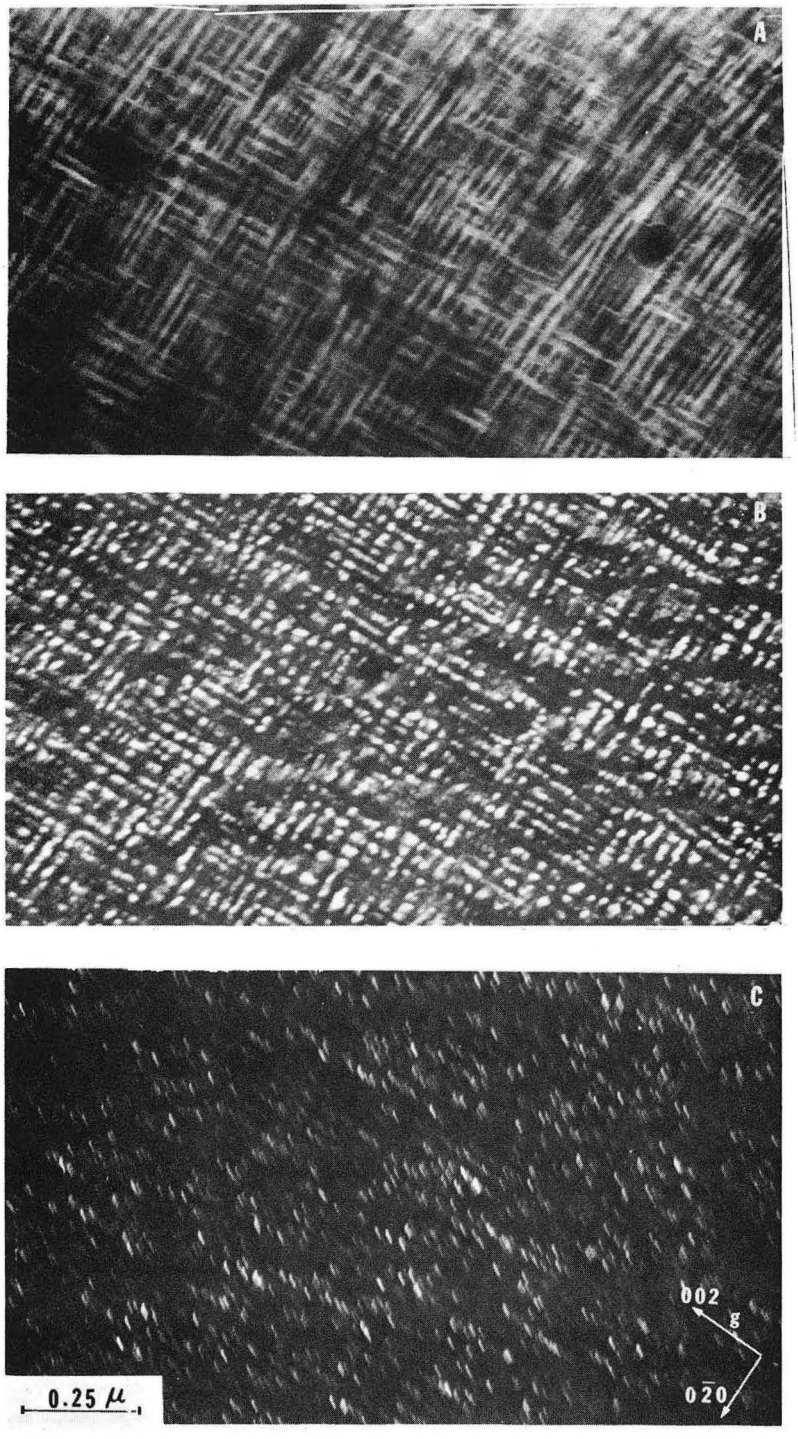

XBB 742-1246

Fig. 12

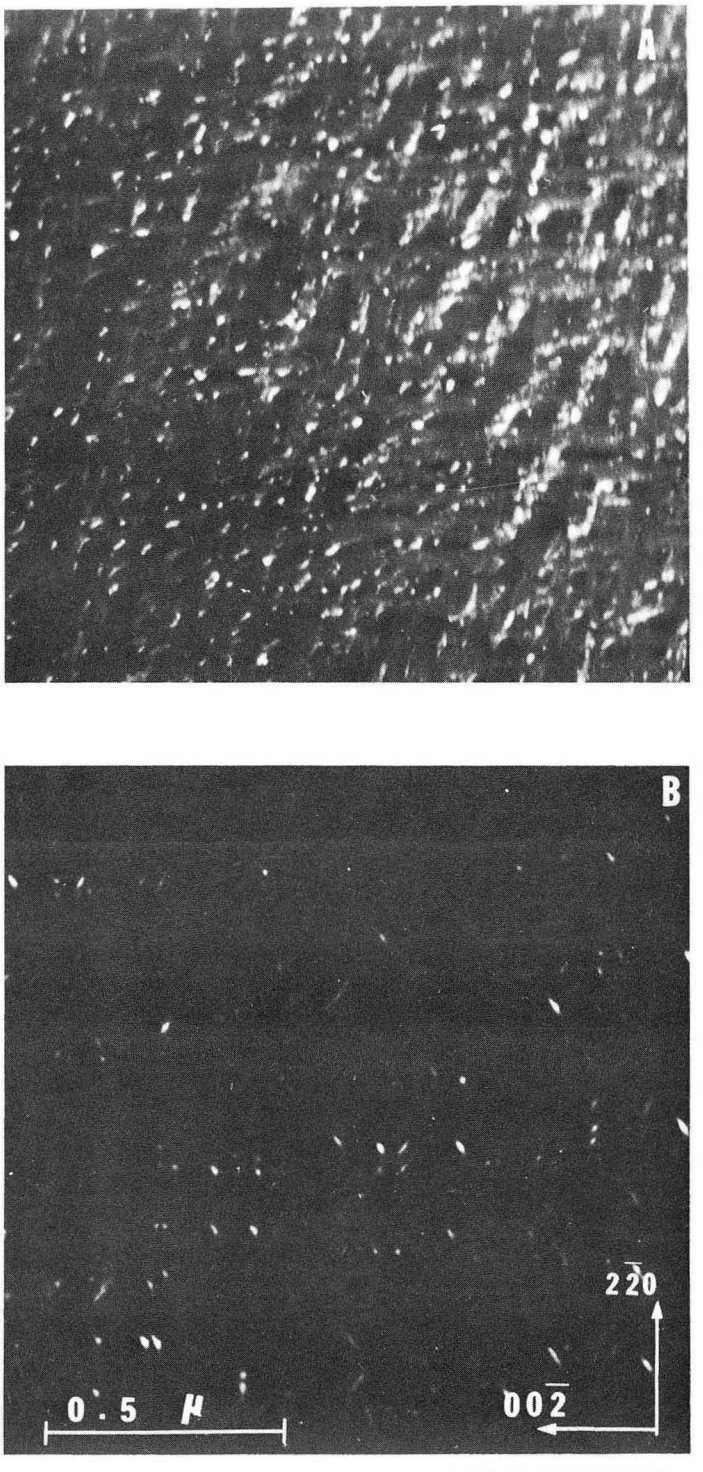

XBB 744-2188

Fig. 13

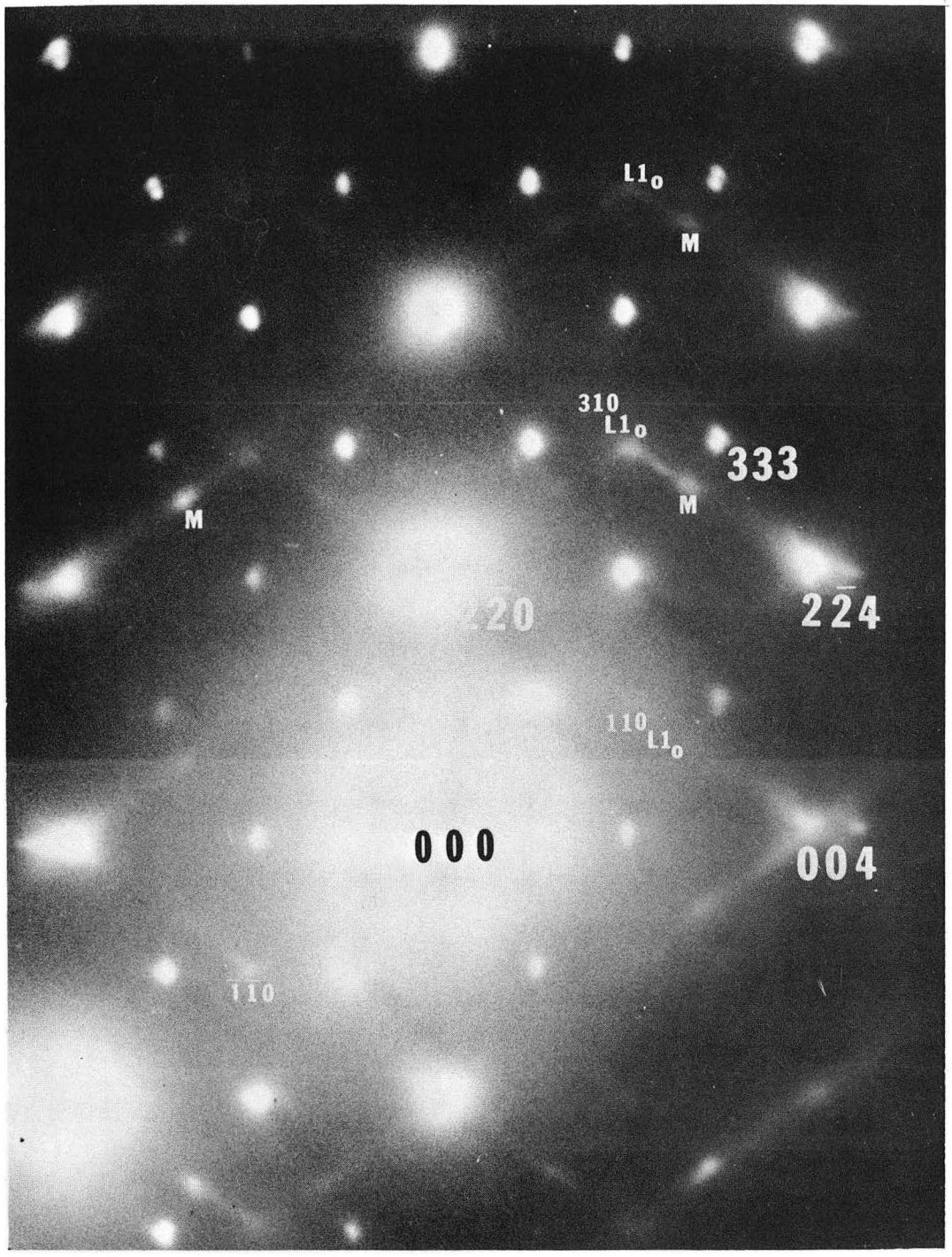

XBB 742-1228

Fig. 14

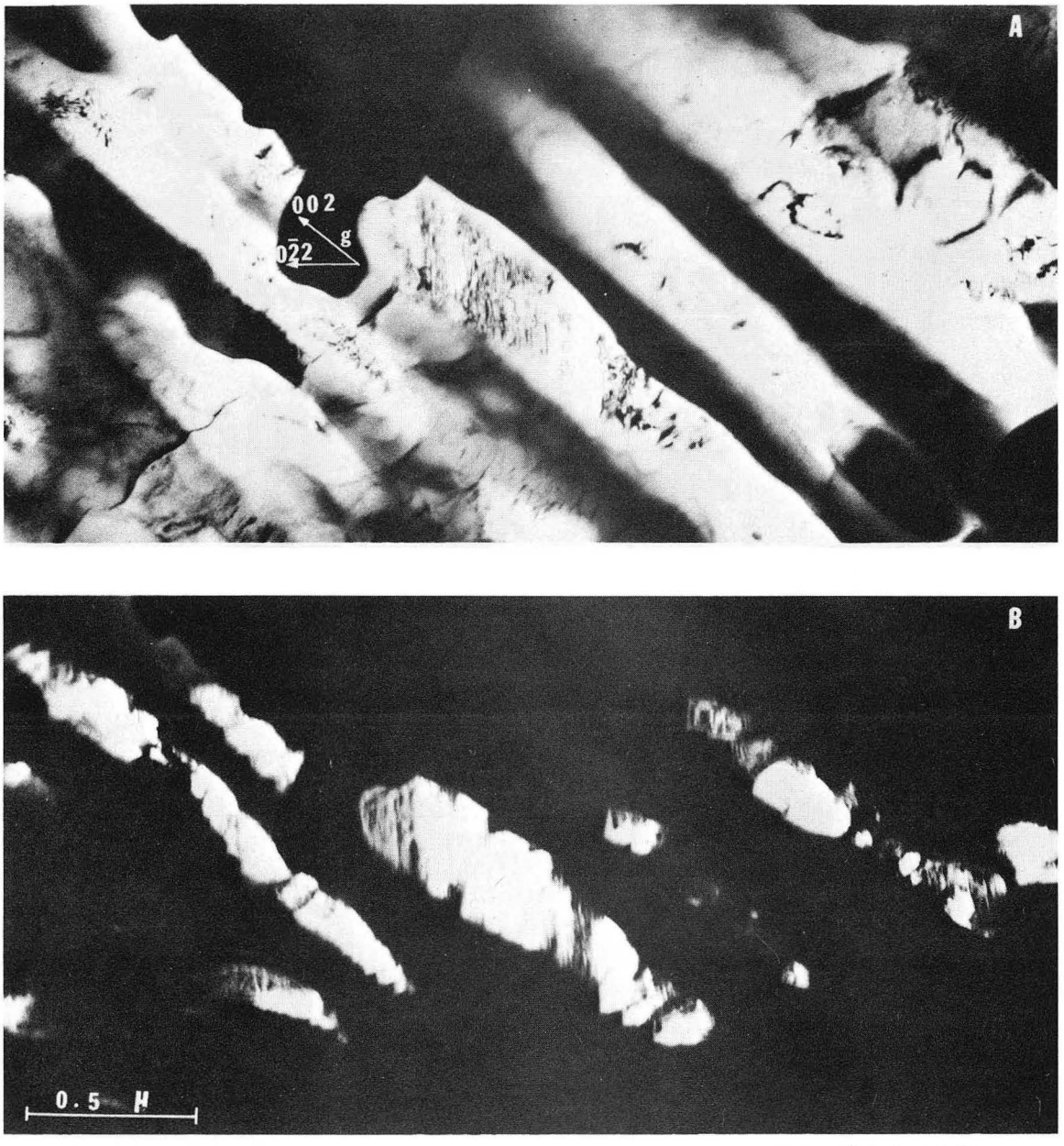

XBB 742-1237

Fig. 15

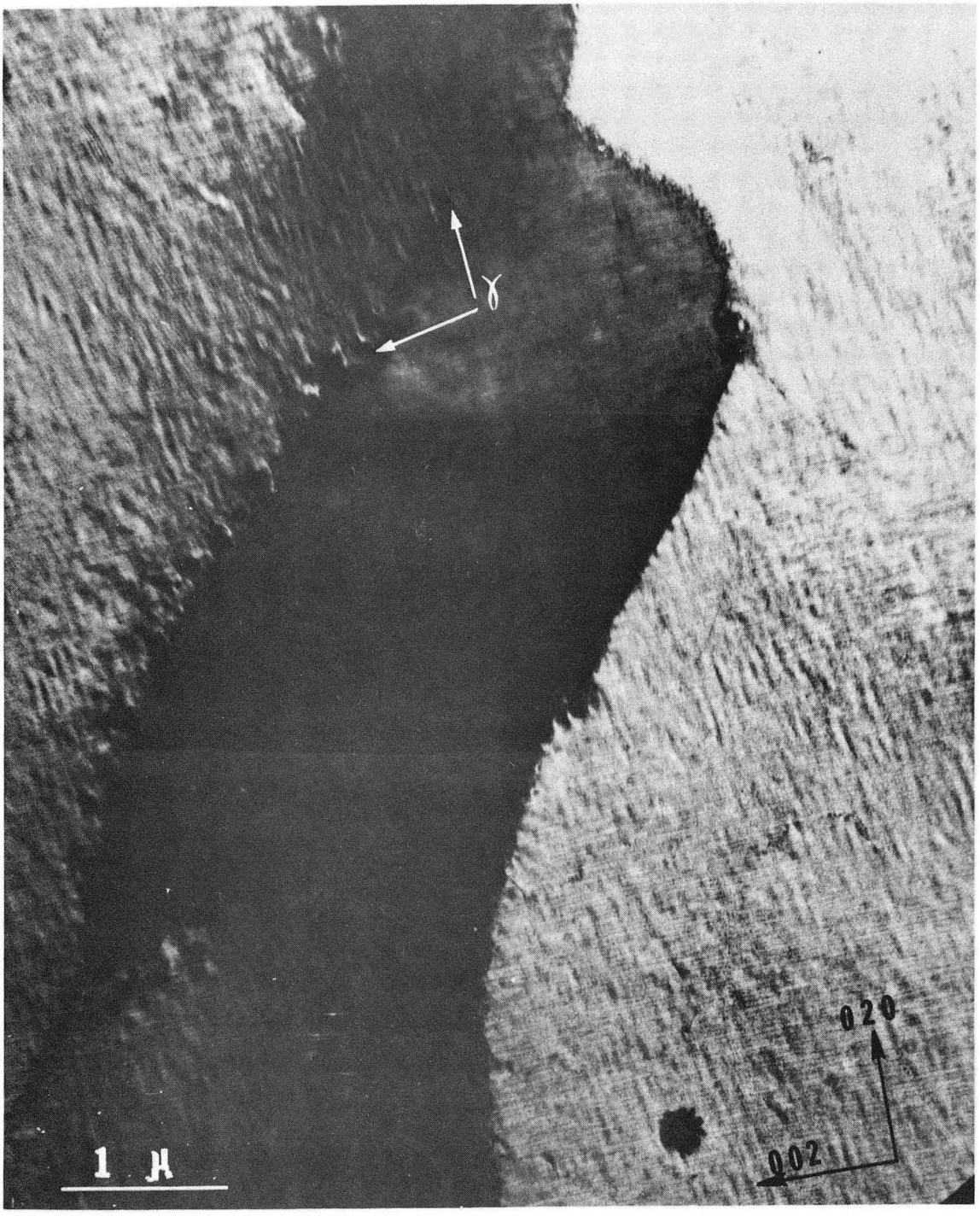

XBB 742-1234

Fig. 16

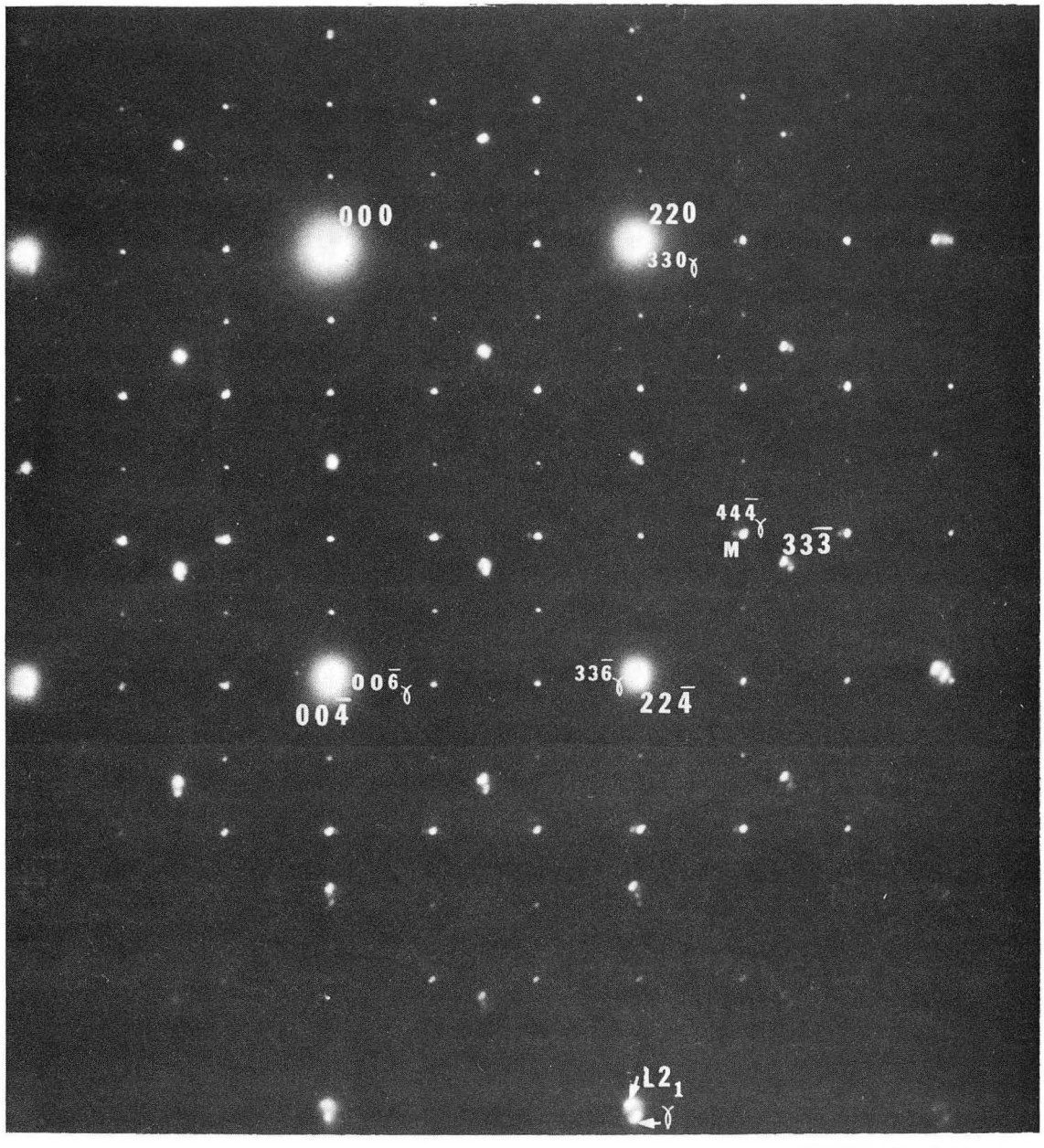

XBB 742-1235

Fig. 17

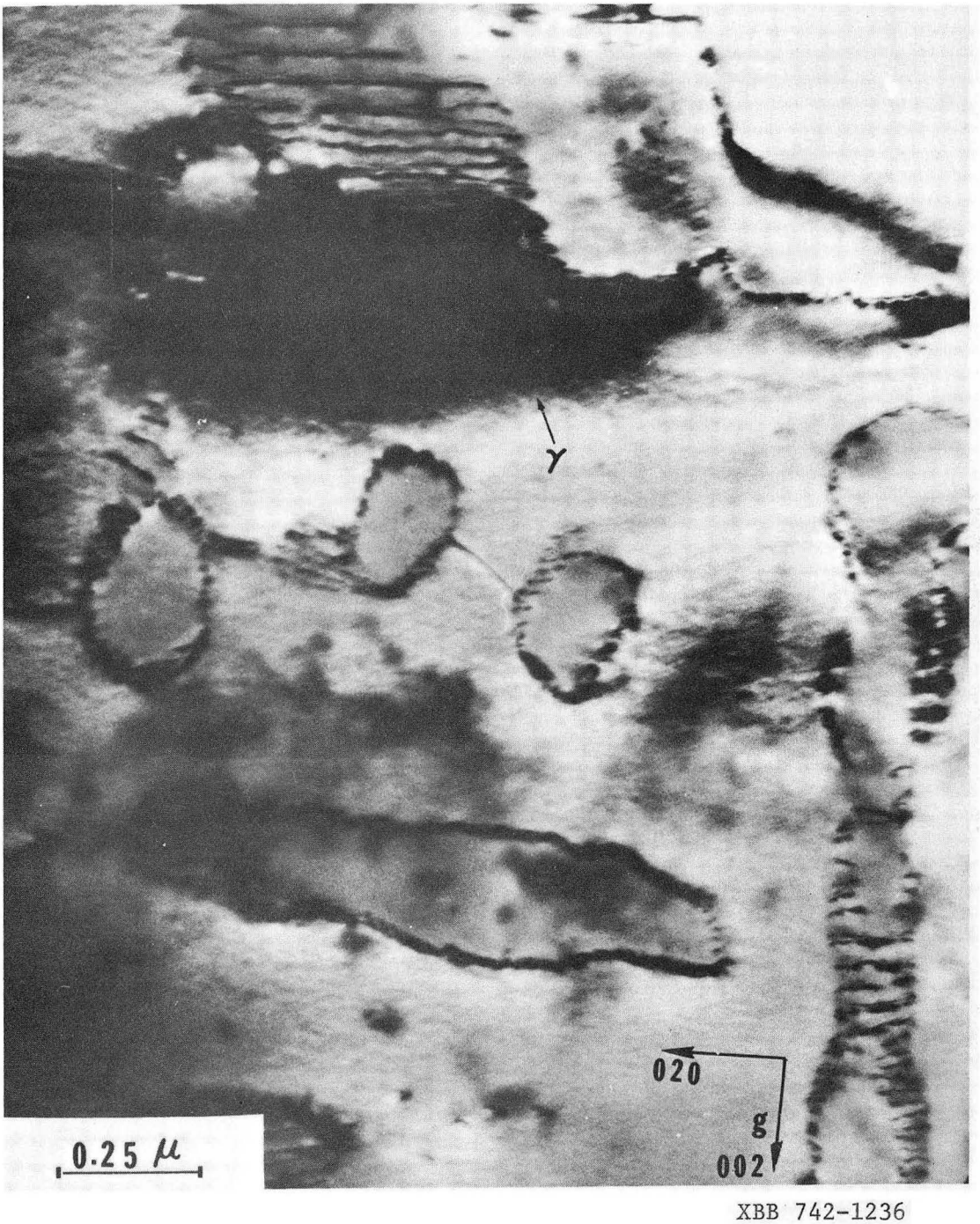

XBB 742-1236

Fig. 18

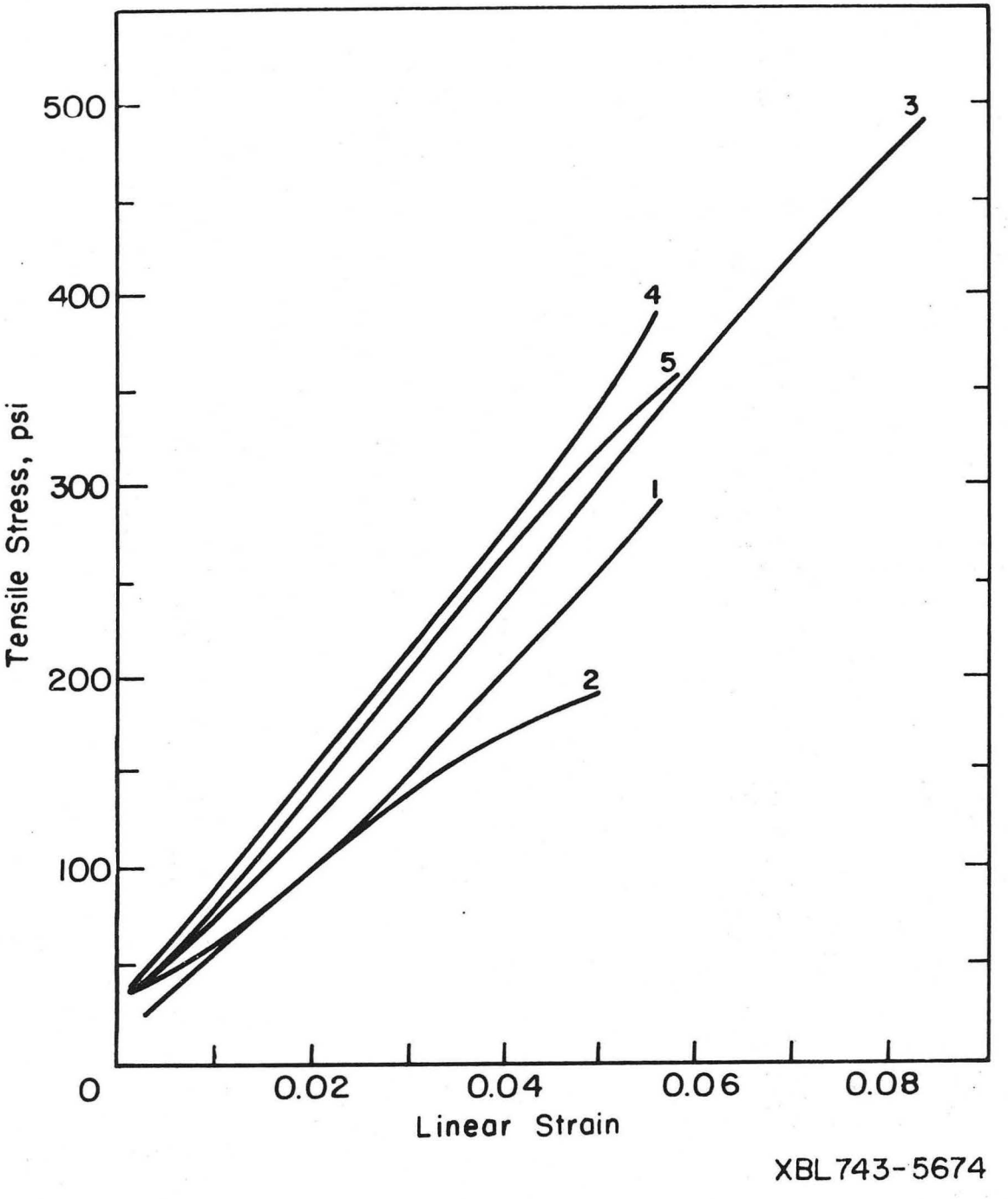
500
400
300
200
100
0
Tensile Stress, psi
0.02
0.04
0.06
0.08
Linear Strain
1
2
3
4
5
XBL743-5674

Fig. 19

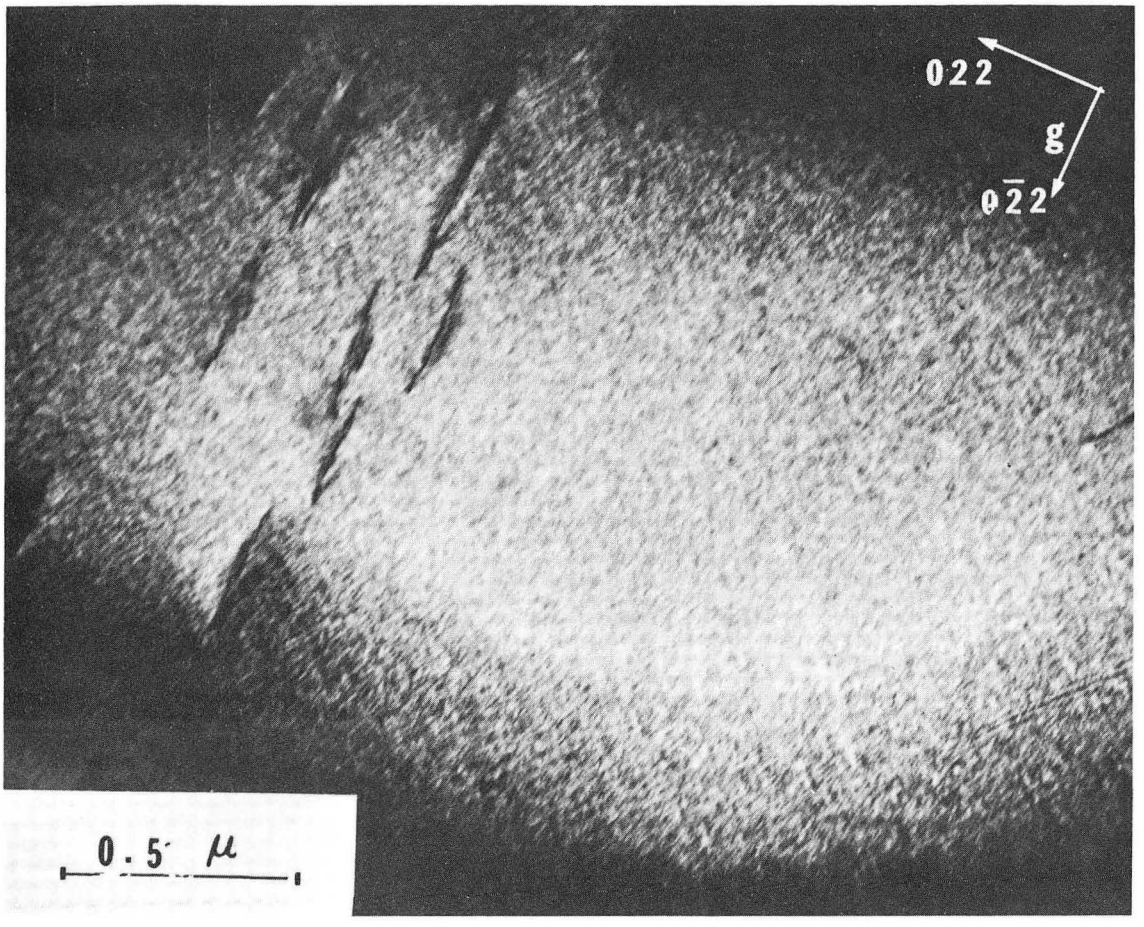

XBB 743-1862

Fig. 20

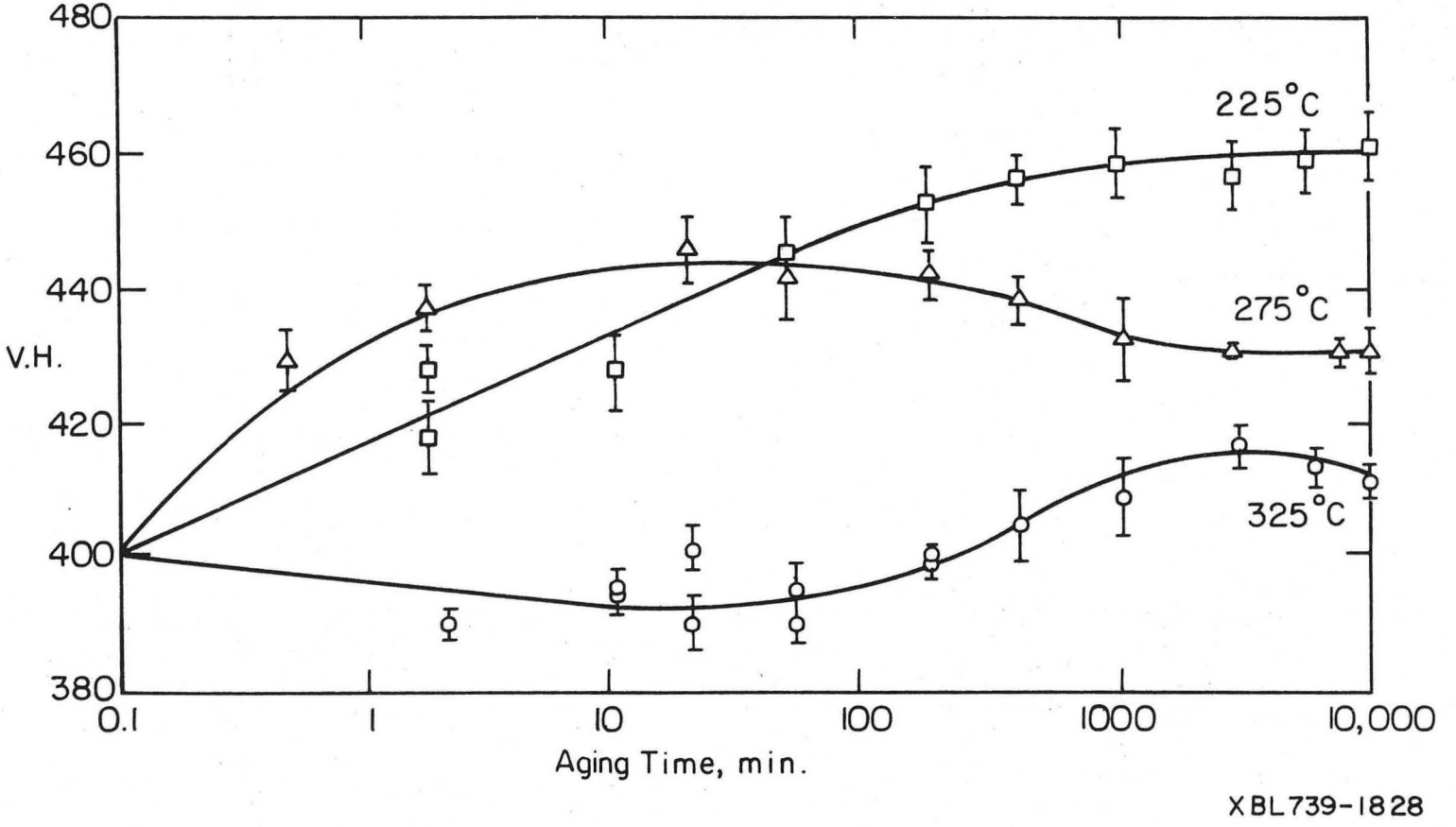
480
460
440
420
400
380
V.H.
225°C
275°C
325°C
0.1
1
10
100
1000
10,000
Aging Time, min.
XBL739-1828

Fig. 21

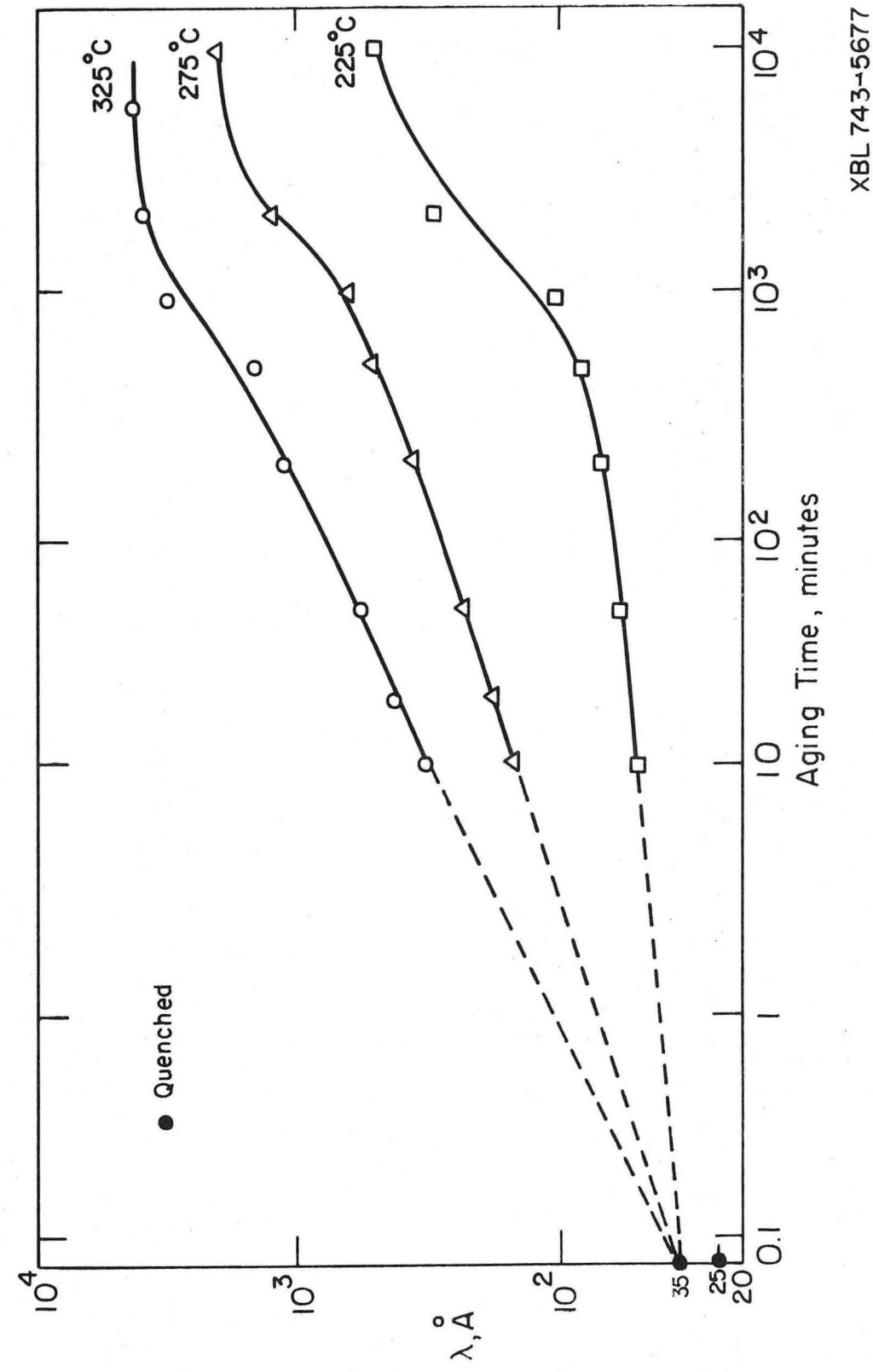

Fig. 22

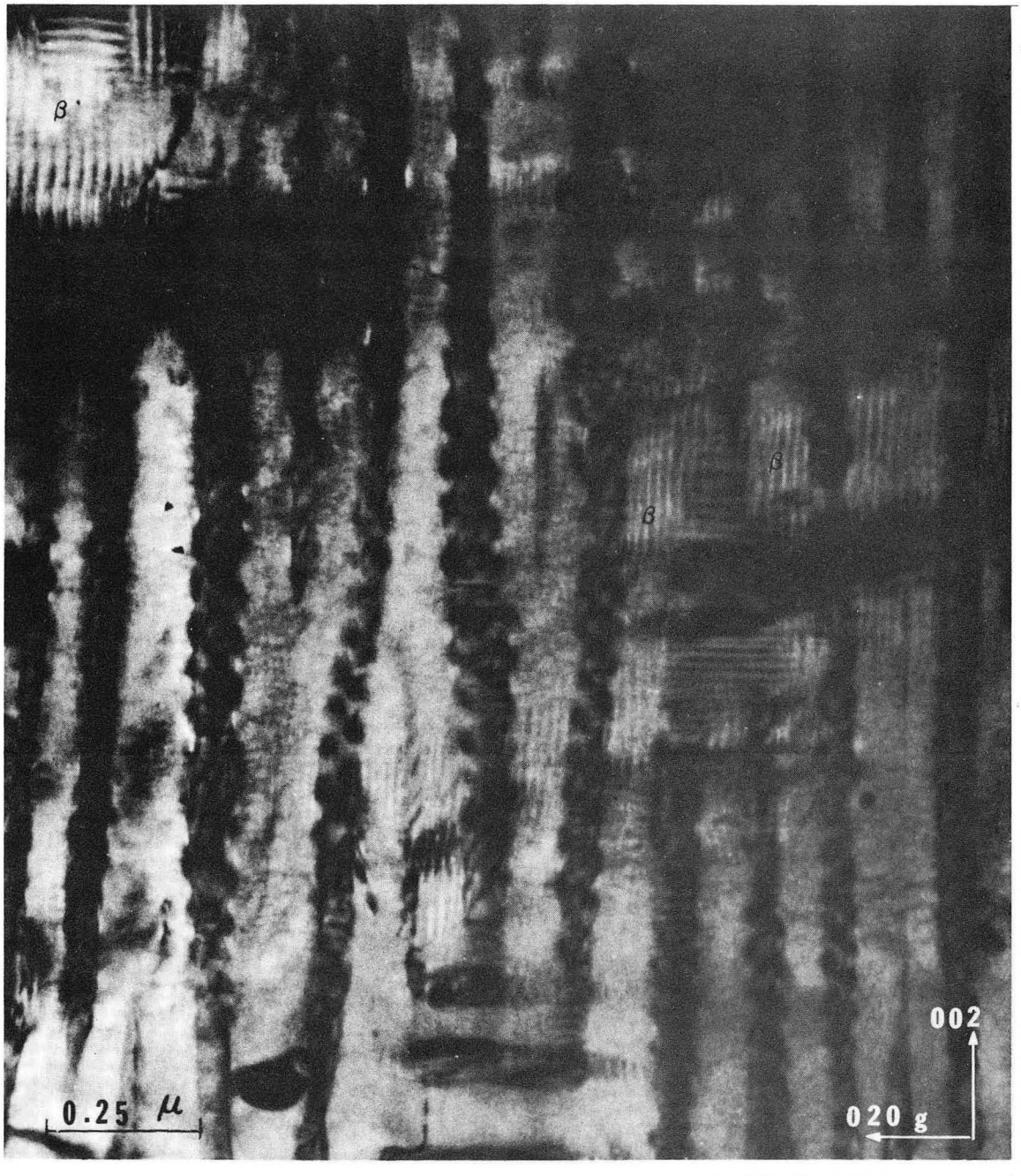

XBB 742-1232

Fig. 23

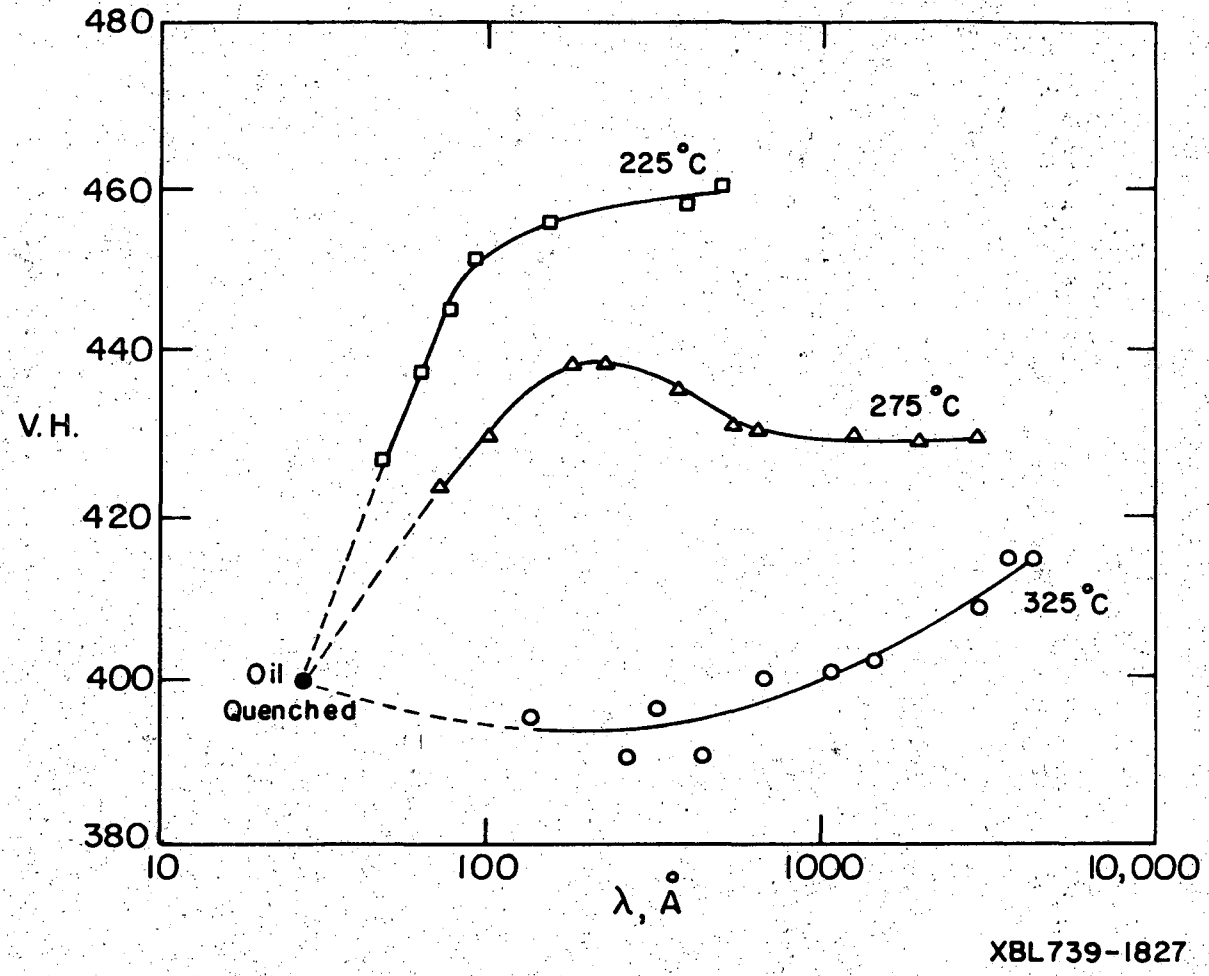
480
460
440
420
400
380
V.H.
225°C
275°C
325°C
Oil
Quenched
10
100
1000
10,000
λ, Å
XBL739-1827

Fig. 24

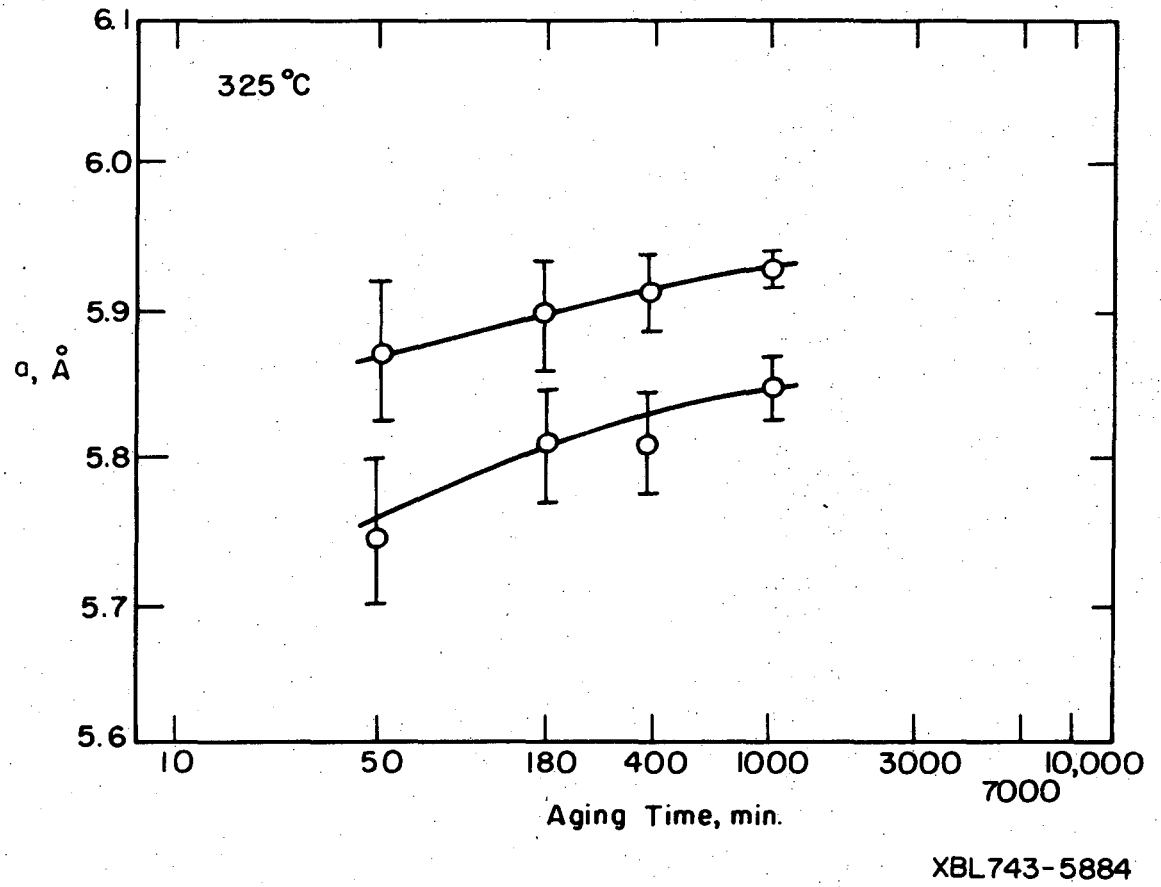
6.1
6.0
5.9
5.8
5.7
5.6
325 °C
a, Å
10
50
180
400
1000
3000
7000
10,000
Aging Time, min.
XBL743-5884

Fig. 25

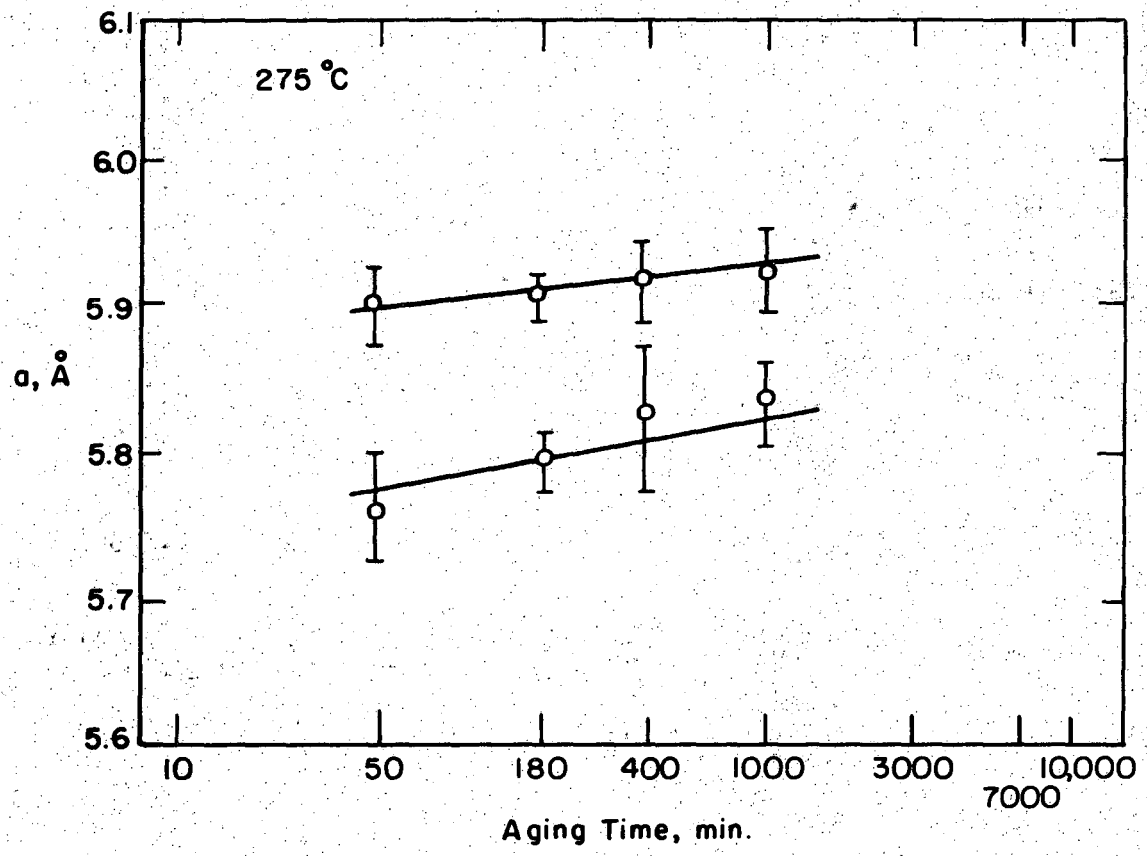
6.1
275 °C
6.0
5.9
a, Å
5.8
5.7
5.6
10
50
180
400
1000
3000
10,000
7000
Aging Time, min.
XBL 743-5883

Fig. 26

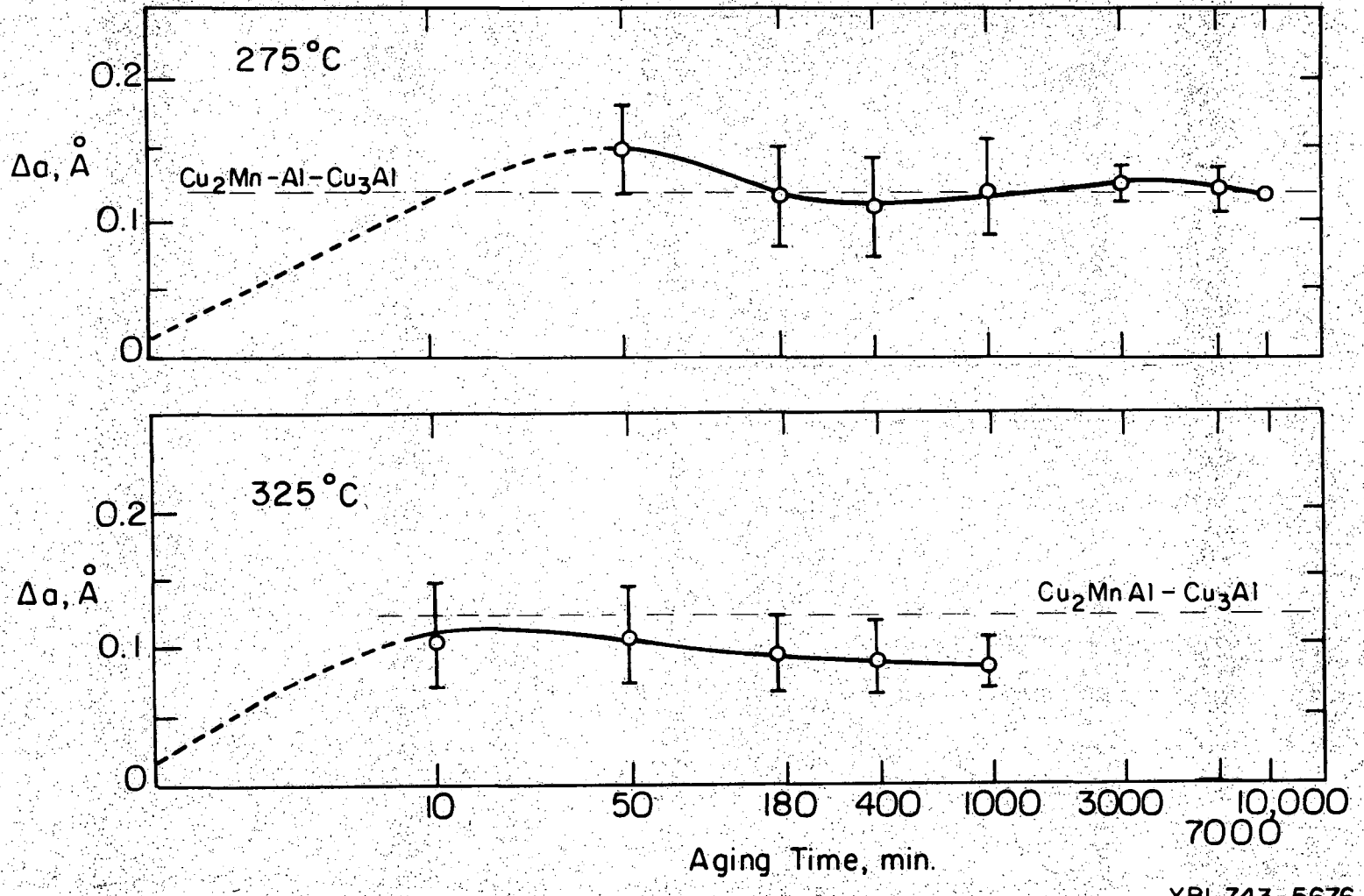

XBL743-5676

Fig. 27

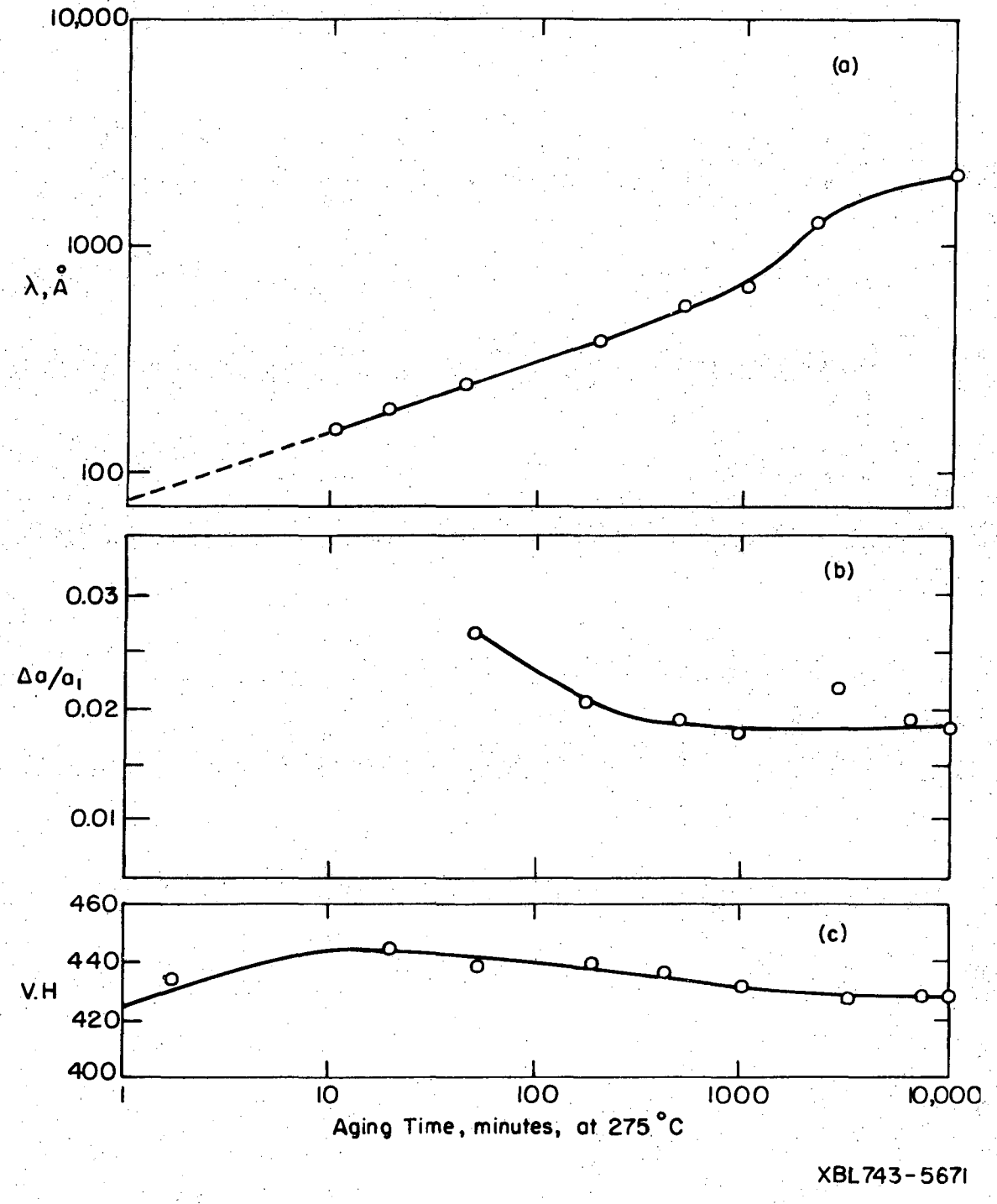
10,000
1000
100
λ, Å
(a)
0.03
0.02
0.01
Δa/a₁
(b)
460
440
420
400
V.H
(c)
1
10
100
1000
10,000
Aging Time, minutes, at 275 °C
XBL743-5671

Fig. 28

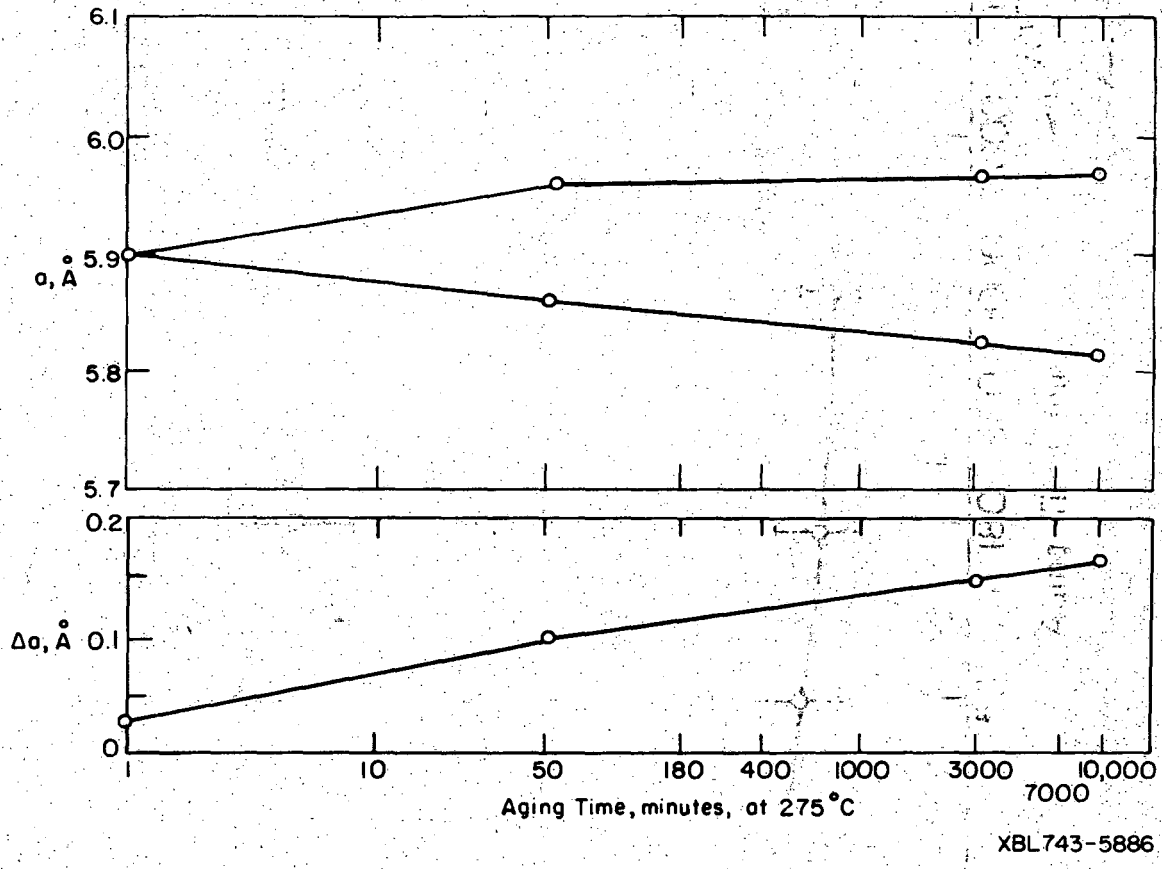
6.1
6.0
a, Å 5.9
5.8
5.7
0.2
Δa, Å 0.1
0
1
10
50
180
400
1000
3000
7000
10,000
Aging Time, minutes, at 275 °C
XBL743-5886

Fig. 29

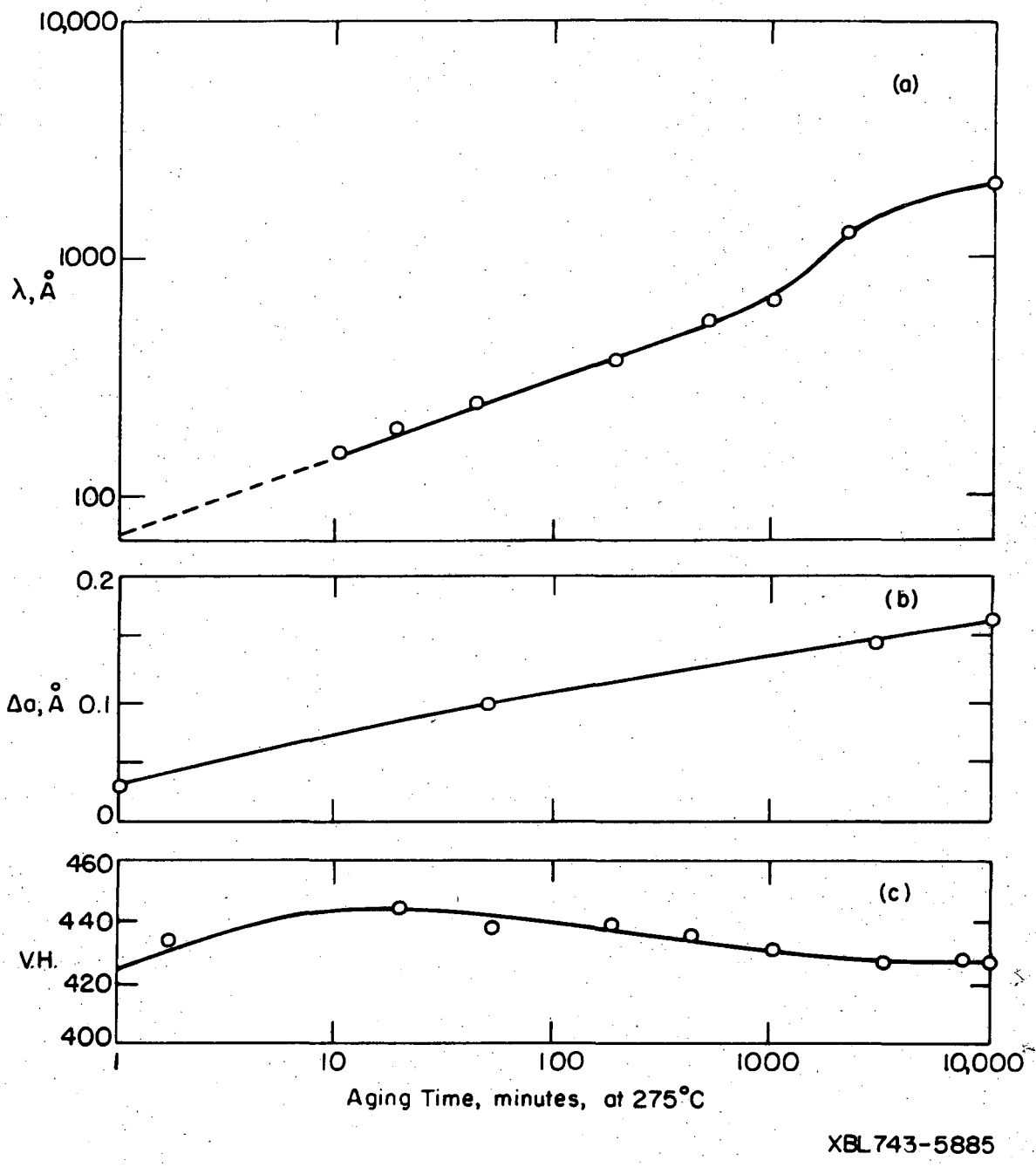
10,000
1000
100
λ, Å
(a)
0.2
0.1
0
Δa, Å
(b)
460
440
420
400
V.H.
(c)
1
10
100
1000
10,000
Aging Time, minutes, at 275°C
XBL743-5885

Fig. 30

LEGAL NOTICE

This report was prepared as an account of work sponsored by the United States Government. Neither the United States nor the United States Atomic Energy Commission, nor any of their employees, nor any of their contractors, subcontractors, or their employees, makes any warranty, express or implied, or assumes any legal liability or responsibility for the accuracy, completeness or usefulness of any information, apparatus, product or process disclosed, or represents that its use would not infringe privately owned rights.

TECHNICAL INFORMATION DIVISION
LAWRENCE BERKELEY LABORATORY
UNIVERSITY OF CALIFORNIA
BERKELEY, CALIFORNIA 94720